GEOGRAPHIC OBJECT-BASED IMAGE ANALYSIS CHANGE DETECTION IN A SHRINKING CITY: DETROIT, MICHIGAN, 2014-2018

by

Vera De Wit
B.A. Hons., University of Toronto 2019

A thesis presented to Ryerson University
in partial fulfilment of the requirements
for the degree of
Master of Spatial Analysis
In the program of
Spatial Analysis

Toronto, Ontario, Canada 2022

Author's Declaration

I hereby declare that I am the sole author of this thesis. This is a true copy of the thesis, including any required final revisions, as accepted by my examiners.

I authorize Ryerson University to lend this thesis to other institutions or individuals for the purpose of scholarly research.

I further authorize Ryerson University to reproduce this thesis by photocopying or by other means, in total or in part, at the request of other institutions or individuals for the purpose of scholarly research.

I understand that my thesis may be made electronically available to the public.

Geographic Object-Based Image Analysis Change Detection in a Shrinking City: Detroit, Michigan, 2014-2018, Vera De Wit, M.S.A., Spatial Analysis, Ryerson University, 2022

Abstract

Over the last several decades, cities in America's Rust Belt region have experienced population and economic declines – most notably, the City of Detroit. With increased property vacancies, many residential structures are abandoned and left vulnerable to degradation. In many cases, one of the answers is to demolish the structure, leaving a physical, permanent change to the urban fabric. The following study uses freely available very high-resolution (VHR) aerial ortho photographs to perform a remote sensing analysis through the application of Geographic Object Based Image Analysis (GEOBIA) methods. The research successfully generates the distinction between pervious and impervious land cover, and links those to parcel lot administrative boundaries within the City of Detroit. Additionally, it explores potential challenges and solutions for batch classification when performing change detection analysis using different sensors at varying spatial resolutions in diverse areas within the city.

Acknowledgements

I would like to extend many thanks to Dr. K. Wayne Forsythe, my supervisor during this research. Thank you for always keeping me on track and guiding me throughout this journey. Thank you to my husband Michael for your unconditional support throughout this work.

Table of Contents

List of Tables

List of Figures

List of Acronyms

ASTER - Advanced Spaceborne Thermal Emission and Reflective Radiometer

CIR - Colour Infrared

DRPS - Detroit Residential Parcel Survey

LULC - Land-Use/Land-Cover

ML - Machine Learning

MODIS - Moderate Resolution Imaging Spectroradiometer

MRS - Multiresolution Segmentation

NAIP - National Agriculture Imagery Program

NIR - Near-Infrared

NDVI - Normalized Difference Vegetation Index

OBCD - Object-Based Change Detection

RT - Random Trees

SPOT - Satellite Pour l'Observation de la Terre

SVM - Support Vector Machine

USGS -United States Geological Survey

USGS EE - United States Geological Survey Earth Explorer

VHR - Very High Resolution

CHAPTER 1: Introduction

1.1 Analysis of Urban Environments Through Remote Sensing

Evaluation of urban conditions and the tracking of changes over time can be performed by ground surveys and visual inspection. These methods can be effective and accurate but can also be time consuming and labour intensive. A second method through which urban environments can be analysed is remote sensing, where ground features are observed from images captured overhead. Additionally, if a phenomenon is not directly recorded, remote sensing archival imagery can be used. Image collection through remote sensing falls into two main categories: airborne and spaceborne. Photographs of Paris were captured from a balloon in 1858—the earliest known example of airborne imagery, and publicly available spaceborne imagery was made available by Landsat-1 in 1972 (Blaschke *et al*., 2014). Medium resolution spaceborne imagery, such as Landsat, is effective in analyzing various land-use/land-cover (LULC) phenomenon in urban contexts (Forsythe and Waters, 2006; Sidhu *et al*., 2016). However, due to the density of features within the urban fabric, higher resolution imagery can display more nuanced information and discrete objects. The most basic analysis of remotely sensed imagery is by simple observation. While much information can be observed by the naked eye, the analysis of pixel spectral values can provide even more detail. For instance, vegetation can be delineated with the help of the red and near infrared (NIR) spectral values. Since the early 2000s, there has been increasing interest in developing new methodologies focusing on analyzing groups of homogeneous pixels, rather than performing pixel by pixel analysis (Hossain and Chen, 2019). This is known as geographic object-based image analysis (GEOBIA), where analysis is performed on objects composed of multiple pixels. Once the spatial resolution of the image displays objects made up of multiple pixels, the ability to conduct analysis pixel by pixel emerges (Blaschke *et al*., 2014). Machine

learning (ML) algorithms such as random tree (RT) and support vector machine (SVM) have been used as classifiers, paving the way for the automation of GEOBIA processes. The combination of higher resolution imagery for analyzing urban environments and the promising potential of GEOBIA make a strong argument for the use of these methods for urban environment analysis.

1.2 Urban Shrinking Phenomenon

In 2018, the United Nations Department of Economic and Social Affairs estimated the global urban population to be 55% and on track to reach 68% by 2050. North America had the highest percentage of urban dwellers, reaching 82% of the total population (United Nations, Department of Economic and Social Affairs, Population Division, 2019). Despite the increasing percentage of urban dwellers, this phenomenon does not translate to uniform urban growth and development. Certain regions and communities experience what is called 'urban shrinking', where there is population decline that often happens in parallel with economic decline. Since the 1950s, about half of America's largest cities have experienced population declines (Hollander, 2011, as cited in Hartt, 2018). According to Thompson and de Beurs (2018), many shrinking cities in the United States are located within the Rust Belt, where property vacancy rates reached 50% in 2012 (Burkholder, 2012). The Rust Belt region is situated in the Great Lakes watershed (Deng and Ma, 2015). However, there is no formal administrative boundary identifying the region. Figure 1.1 displays an informal boundary based on analysis of characteristics by Thompson and de Beurs (2018).

Figure 1.1: Rust Belt region, based on analysis by Thompson and de Beurs (2019).

1.3 Research Objectives

The purpose of this study is to test the feasibility of using open-source airborne imagery for detection of changes in shrinking urban environments—specifically, demolished residential structures in Detroit. Shrinking urban areas may lack quality parcel data (Deng and Ma, 2015), and in many cases, parcel lot vacancy statistics are not available (Biron, 2022). Acquiring imagery from high-resolution commercial satellites for a city-wide analysis can be prohibitively expensive (Thompson and de Beurs, 2018). This study aims to build upon GEOBIA methodologies such as image segmentation and object classification and develop a semi-automated method for analysis

of large urban areas captured via different sensors, and at different times. The method is then tested as a proof of concept on three levels of change due to demolition rates: high, median, and low. The research questions are:

(a) What are the optimal image segmentation parameters for delineating surfaces under shadows in this study?

(b) What is the effectiveness of developing a segmentation and classification method and applying it to different areas of Detroit?

(c) Does the same method produce appropriate results when applied to imagery from different dates, sensors, pixel resolutions, and spatial locations for the purpose of repeatability?

(d) Can accurate parcel lot classification occur? What valuable information can be extracted with the achieved change detection accuracy?

CHAPTER 2: Literature Review

2.1 Geographic Object-Based Image Analysis

2.1.1 Origins

Fields such as computer vision, material sciences and biomedical imaging use object-based image analysis (OBIA) methodologies (Blaschke, 2010). Hay and Castilla (2008) stress the importance of distinguishing spatial applications of OBIA and calling it geographic object-based image analysis (GEOBIA) when applied to remote sensing. OBIA concepts have been present in research since the 1980s, but not widely used in geographic research until the early 2000s (Blaschke, 2010). The advancement of high-resolution imagery in combination with off-the-shelf OBIA software led to interest in GEOBIA applications for various research questions (Blaschke, 2010). Launched in 2000, eCognition was the first commercially available GEOBIA software, and remains popular among researchers to this day (Ma *et al*., 2016; Mendiratta and Gedam, 2018; Maxwell *et al*., 2019; Norman *et al*., 2021; Toney *et* al., 2012; Yen *et al*., 2020). One of the driving forces that encouraged the development of GEOBIA research was to provide a method for analyzing high resolution imagery (Lang, 2008 cited in Hossain and Chen, 2019; Mendiratta and Gedam, 2018; Johnson and Ma, 2020). Johnson and Ma (2020) also highlight the spread of GEOBIA applications to low and medium resolution research, suggesting greater potential for the method across different research applications.

2.1.2 Components of GEOBIA

Classification applications through GEOBIA have the following components: "(a) image segmentation, (b) object hierarchy development (based on training data set), and (c) classification" (Hussain *et al*., 2013).

The first step is segmenting the image into image-objects. This is arguably the most important element, as it determines the quality and accuracy of the analysis (Johnson and Ma, 2020). Commercially available software such as eCognition and CATALYST Professional's Object Analyst perform multiresolution segmentation (MRS), using multiple parameters to influence the segmentation output. MRS uses scale, shape, and compactness as parameters (Norman *et al*., 2021), to define the desired outcome of the image-objects when segmenting the image. Scale represents the size of the desired objects, the shape is a weight metric that is inversely proportional to the importance of the pixel value, and compactness represents the weight metric which determines how compact the desired objects will be (Maxwell, 2010). Additionally, there is an option within Object Analyst to select one or more of the channels on which the segmentation is performed. Within segmentation algorithms, the scale impacts the size of the segmented objects (Hussain *et al*., 2013). However, objects appear differently when displayed with different resolutions, making it challenging to predict the proper scale in advance (Blaschke, 2010). The question of what scale is appropriate for what object is yet to be answered (Hossain and Chen, 2019). Maxwell *et al.* (2019) indicates that scale is the most significant of the three parameters. Classification of segmented image-objects can be either unsupervised, such as K-Means clustering, or supervised, where training is required and algorithms, like RT and SVM, are used.

2.1.3 Object-Based Change Detection

Change detection can be described as "the process of identifying differences in the state of an object or phenomenon by observing it at different times" (Singh, 1989). Object-based methods extend this definition to "the process of identifying differences in geographic objects at different moments using object-based image analysis" (Chen *et al*., 2012). Hussain *et al*. (2013) describe

three object-based change detection (OBCD) techniques: direct object change detection, classified objects change detection, and multitemporal/multidate-object change detection. Direct object change detection refers to comparing objects' boundaries and/or the attribute values within the object's boundary. Classified objects change detection is the practice of classifying objects into classes, which can later be used for from-to comparison. Finally, multitemporal/multidate-object change detection incorporates stacks of images in the method. Urban objects have discrete boundaries, making OBCD techniques appropriate for urban change detection (Chen *et al*., 2012).

2.1.4 Advantages and Disadvantages

Image analysis in remote sensing is traditionally performed with pixel-based methods (Wang *et al*., 2018). With GEOBIA, the classification is performed on the properties of the objects, rather than individual pixels (Toney *et al*., 2012). Image-objects can contain statistical values of the spectral properties, as well as geometrical attributes such as rectangularity, circularity, and elongation. Performing classification of image segments over individual pixels is commonly cited as improving the salt and pepper effect, where pixels are misclassified and appear as specks in incorrect classes. Mendiratta and Gedam (2018) demonstrated the reduction of the salt and pepper effect in a medium resolution urban analysis, and multiple review articles indicated the potential for the issue to be resolved by GEOBIA (Blaschke, 2010; Hussain *et al*., 2013). The second often-cited benefit of GEOBIA over pixel-based approaches is the generation of vector data (Blaschke, 2010), which can be more easily integrated with other vector types of data for further geographic information analysis. Discrete objects are especially "useful for thematic mapping and change detection" (Hussain *et al*., 2013). The third advantage of GEOBIA over pixel-based approaches is particularly important when performing time series analysis with very high-resolution imagery.

There is a risk of pixel mis-registration when using very high resolution (VHR) imagery and classifying multiple pixels as an object can reduce the error impact (Maklea and Pekkarinen, 2001, cited in Chen *et al.,* 2012). The first disadvantage of using GEOBIA methods is the user experience. In a questionnaire sent to authors of GEOBIA research, many indicated the lack of 'user friendly' software (Johnson and Ma, 2020). Secondly, since image segmentation parameters are left to the analyst's discretion, there is potential for experimental approaches that introduce bias. This directly impacts the image segmentation results, which influences the overall classification. Thirdly, computational requirements can become a challenge when processing VHR imagery over large spatial extents (Maxwell *et al.*, 2019).

While there are advantages and disadvantages for using GEOBIA approach over pixel-based methods, the application of GEOBIA methods can be more useful when the task is to identify discrete objects, and pixel-based approaches can be more useful for classify LULC.

2.2 Study Area and Previous Urban Analysis

Detroit is in the American State of Michigan and borders Windsor, Ontario, Canada. The city covers over 370 square kilometres (United States Census Bureau, 2021), and is home to 639,111 residents (United States Census Bureau, 2020), making it the largest city in the state by area and population. Detroit was chosen for the analysis and proof-of-concept implementation for two reasons: (a) there is a strong foundation of ancillary data that can be used for validation purposes, and (b) it is a one of the largest and most notable examples of a shrinking city with active, intensive demolition efforts, representing the type of urban fabric across the Rust Belt region that might experience similar shrinking phenomenon on a smaller scale (Xie *et al.* 2018).

2.2.1 Detroit's Decline

After establishing itself as the world's automotive capital in the early 20th century, the city experienced rapid population growth (Figure 2.1). Detroit's population reached its peak in the 1950s with over 1.8 million inhabitants, making it the fifth largest city in the United States at the time (Gibson, 1998). Since then, Detroit's population has consistently declined each decade, with less than half of its peak population currently remaining. Some attribute the beginning of Detroit's decline to the race riots of 1967 (Ager, 2015; The Economist Newspaper, 2017a; The Economist Newspaper, 2017b), and migration to the suburbs. Additionally, the city has experienced economic disruption caused by decentralization, automation of heavy industry and manufacturing, and foreign competition (Hoalst-Pullen *et al.*, 2011). In a study evaluating population and economic metrics of the 20 largest American cities that lost population between 1980-2010, Hartt (2018) identified Detroit as undergoing both population and economic decline. With this decline over time, many residential structures were abandoned and left vacant, exposing them to decay and vulnerable to scavenging. Vacant structures deteriorated to the point of endangering adjacent communities (Xie *et al*., 2018), and in some instances resulted in safety concerns (Kinder, 2016, cited by Foster and Newell, 2019). Between 1970 and 2000, over 160,000 housing units were demolished in Detroit (Goodman, 2004), and based on a city-wide parcel survey published in 2014, 112,000 lots were estimated to be vacant (Data Driven Detroit, 2014a). In 2016, the city's vacant land was estimated to be approximately 60 square kilometres (Detroit Future City, 2016). Detroit's continuous decline led to it filing the largest American municipal bankruptcy in 2013, worth over $18 billion. Shortly after the bankruptcy in 2014, Mike Duggan was elected mayor and oversaw efforts to eradicate urban blight. Despite previous promises of demolition for many years (Byles, 2006), actual work between 2014 and 2020 resulted in over 21,000 residential structures being

demolished (City of Detroit, 2021) (Figure 2.2). Cities are dynamic in their nature, and Detroit is a prime example of changes occurring in a shrinking city.

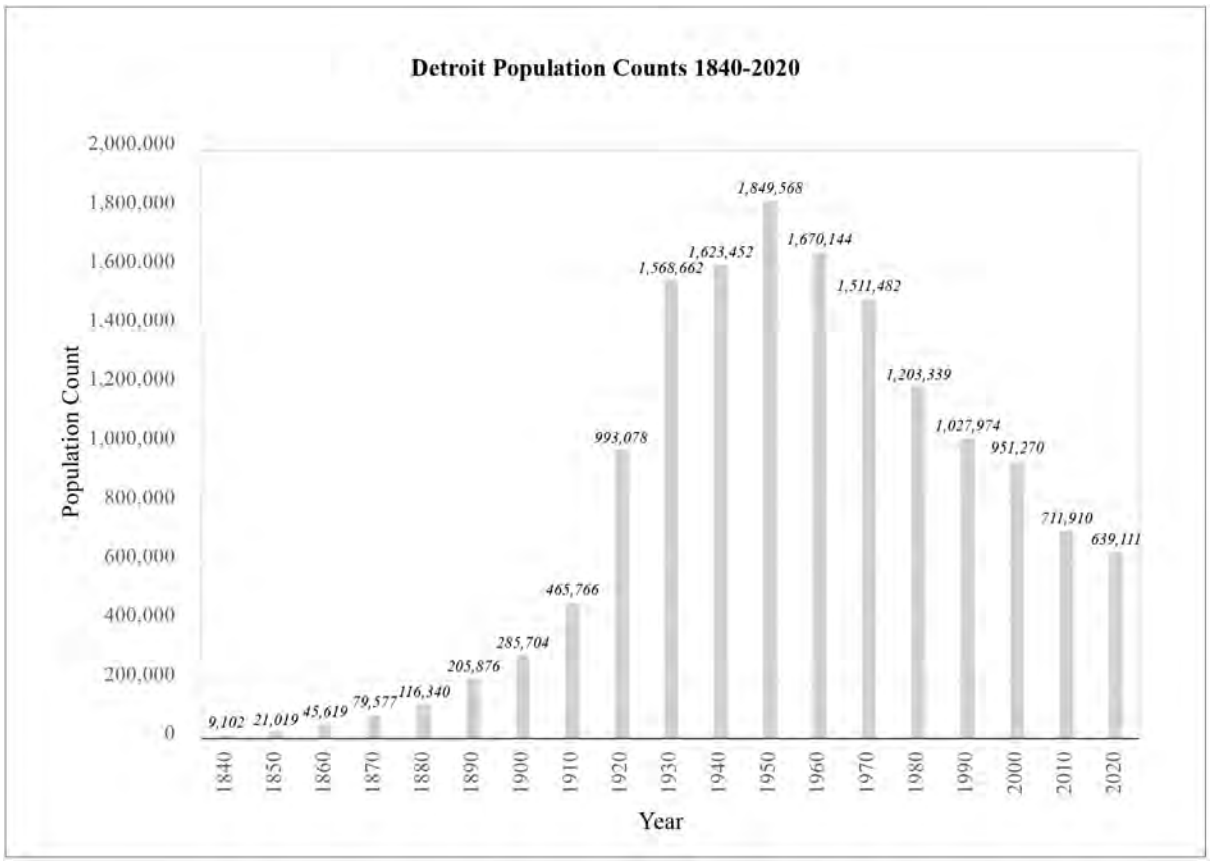

Figure 2.1: Detroit Population Counts, 1840-2020

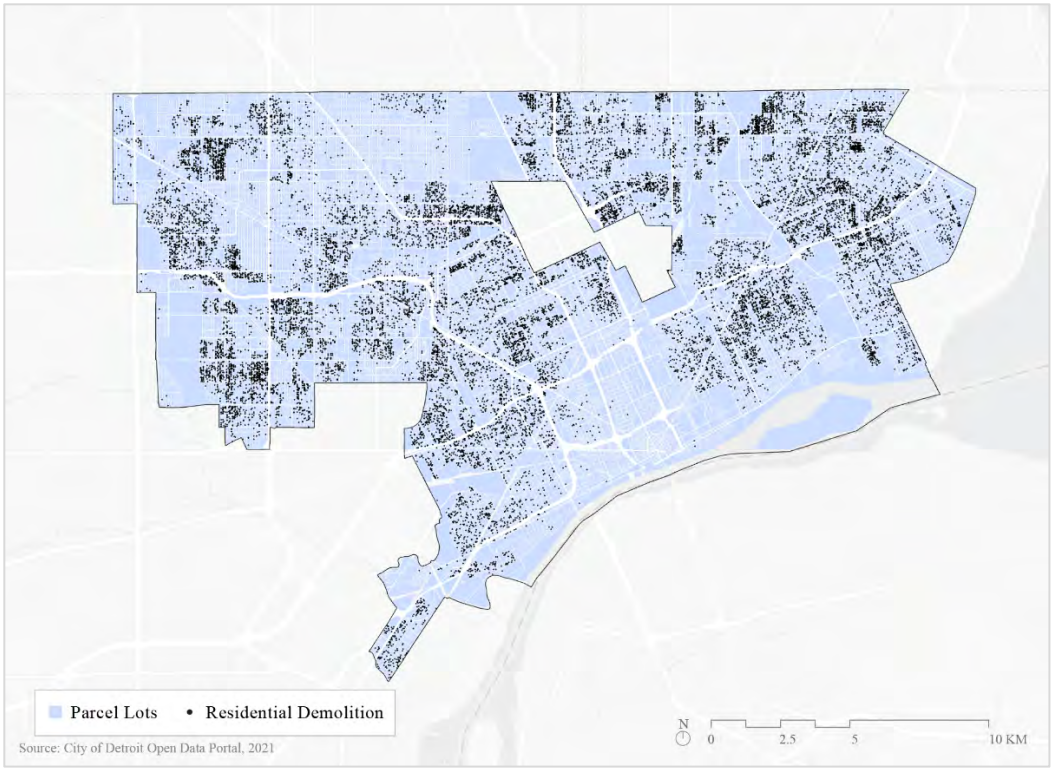

Figure 2.2: Complete Residential Demolitions 2014-2018

2.2.2 Urban Shrinking Analysis in Detroit

Much of the urban change analyzed through remote sensing has focused on urban growth, often ignoring urban shrinking (Thompson and de Beurs, 2018). The condition of features detected, such as deteriorating rooftops, may require a unique approach when analysing change. While research has evaluated and attempted to predict residential vacancies by correlating vegetative growth on lots and incorporating remotely sensed data as part of the analysis (Deng and Ma, 2015), fewer studies have been conducted purely on lot vacancy. Residential vacancy refers to the absence of a residence on a lot, with or without structure (Deng and Ma, 2015), while lot vacancy refers to the absence of structures on the lot. As previously mentioned, Detroit's population has been under continuous population and economic decline, resulting in a long history of structure demolition. Recently, two major surveys evaluated parcel lot conditions in Detroit: (a) the Detroit Residential Parcel Survey (DRPS) in 2009 and (b) the Detroit Parcel Survey: Motor

City Mapping in 2014. The DRPS was conducted in the summer of 2009, where teams of three drove around Detroit and visually surveyed each residential property with four or fewer units (Detroit Data Collective, 2010). According to this survey, 26% of residential parcel lots were vacant at the time. The Motor City Mapping survey conducted city wide on all use zones also gathered information on parcel lots. About 190 surveyors and volunteers evaluated each parcel and the structures present on site (Data Driven Detroit, 2014b). According to the first round of surveys, over 112,000 parcel lots were vacant. In both cases, the surveying efforts were resource intensive and required a large amount of human capital. Based on the two studies outlined above, Thompson and de Beurs (2018) performed a city-wide analysis of parcel lot vacancy between 2009-2014, with the use of airborne Light Detection and Ranging (LiDAR). The research was based on classifying parcel lots and performing a change detection matrix based on the classification.

2.3 Airborne Imagery

Various remote sensing applications have used spaceborne acquired imagery, when applied to land-use/land-cover (LULC) mapping. Blaschke (2010) refers to Landsat, Satellite Pour l'Observation de la Terre (SPOT), Advanced Spaceborne Thermal Emission and Reflective Radiometer (ASTER) and Moderate Resolution Imaging Spectroradiometer (MODIS) satellites as the "work horses". However, their images are too coarse to detect individual objects within the urban context. For instance, a single 30m Landsat 8 pixel contains 2,500 0.6m aerial National Agriculture Imagery Program (NAIP) pixels (Figure 2.3). When performing an analysis with VHR imagery, one of the aims is to balance usable spatial resolution with computational capacity. Higher resolution is not equivalent to 'better' identification results. With the improvement of 1m

resolution satellite imagery such as IKONOS (launched in 1999), smaller features in the urban environment can be detected. However, as mentioned above, acquiring imagery from commercial satellites can be expensive, and preforming an analysis on large spatial extents may require large amounts of storage and computational capacity.

Airborne imagery has been used in various urban environmental analyses. Thompson and de Beurs (2018) analyzed parcel vacancy in Youngstown, New York with orthophotos of one and 0.5 foot resolution. Deng and Ma (2015) calculated the Normalized Difference Vegetation Index (NDVI) within parcel lot boundaries from one foot resolution colour infrared (CIR) photographs in the Triple Cities Region of New York. Ginner *et al*. (2013) used 0.5m CIR aerial imagery to detect lawns across 26 towns in northeastern Massachusetts. Merry *et al*. (2014) performed urban tree canopy change detection in Detroit and Atlanta by utilizing one metre colour infrared NAIP imagery, and aerial photographs from 1951. Ellis and Mathews (2019) performed an object-based delineation of the urban tree canopy in Oklahoma City by using LiDAR derived data in conjunction with NAIP one metre imagery.

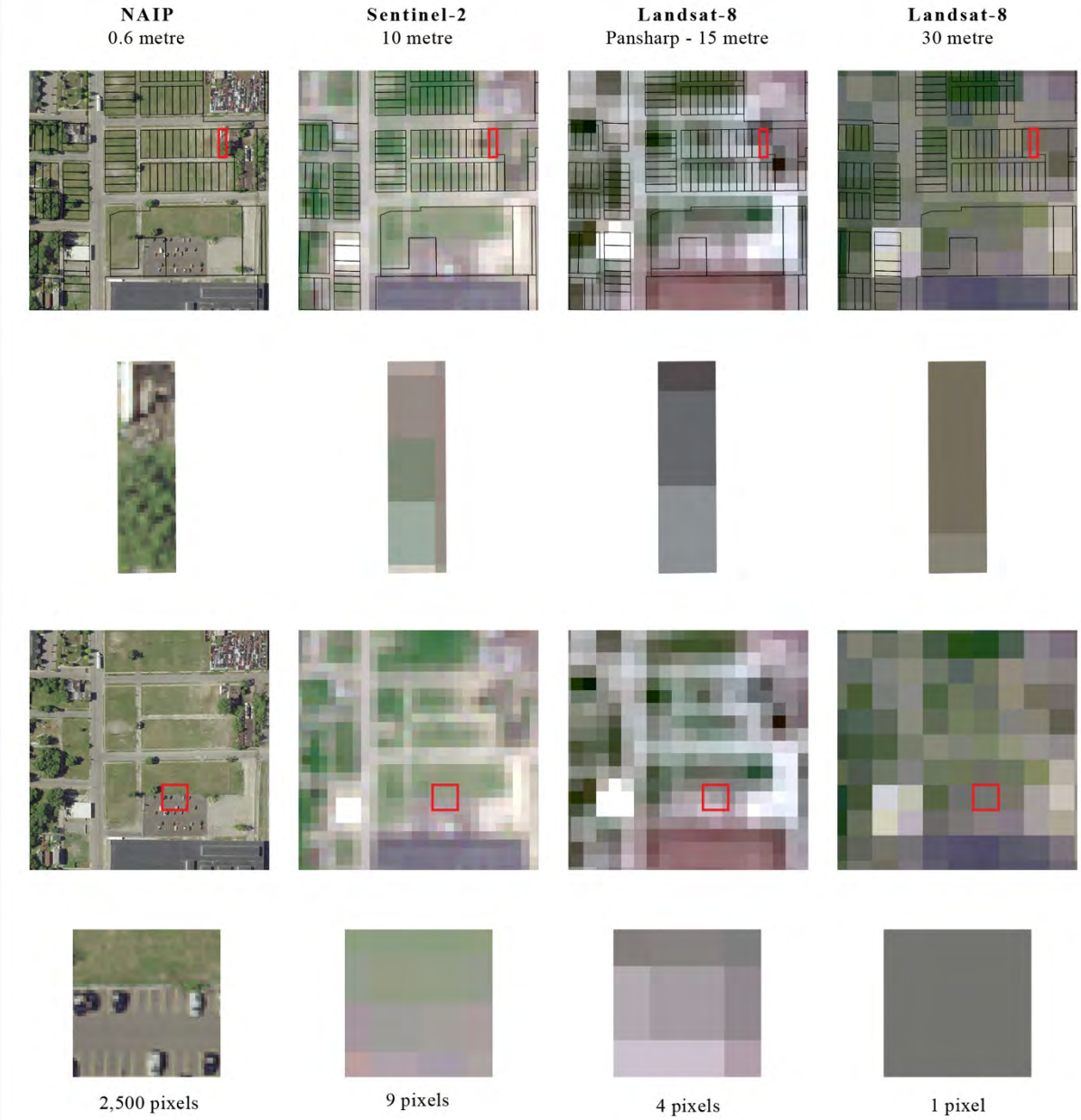

Figure 2.3: Pixel comparison.

2.3.1 National Agriculture Imagery Program

NAIP imagery is managed by the United States Department of Agriculture Farm Service Agency (USDA-FSA), and has captured the continental United States since 2003, with a maximum three-year gap in collection (United States Department of Agriculture, 2021). The imagery is

orthorectified and formatted to a 3.75-minute longitude by 3.75-minute latitude quarter quadrangle tile (Davis, 2017). Acquisition time matches the agricultural growing season, resulting in imagery rich with vegetation. Additionally, NAIP imagery claims to contain no more than 10% cloud cover per tile (United States Department of Agriculture, 2021). Despite NAIPs origin in agriculture, its VHR imagery has been used in various remote sensing analysis, such as the urban environments listed above.

CHAPTER 3: Data

3.1 Raster Imagery

This study's timeline was defined by the acquisition dates of the NAIP imagery available through the United States Geological Survey Earth Explorer (USGS EE) website. The first set of imagery was acquired on June 28, 2014, and the second set between July 6-7, 2018. The images contain an eight to nine calendar-day difference, however due to NAIP's aim of capturing vegetative peak, this difference is assumed to be acceptable. For simplicity, this study refers to the first imagery dataset as NAIP 2014 and the second imagery dataset as NAIP 2018. While both sets of imagery are CIR, the resolution differs, where NAIP 2014 is at one metre and NAIP 2018 is at 0.6m. According to the metadata provided with the imagery file, the acquisition sensors and flight altitudes are different (Table 3.1). Additionally, the time of acquisition was different, resulting in opposing directions of shadows. To cover Detroit's administrative boundary, 22 tiles were downloaded in May 2021, and stitched using the CATALYST Professional Mosaic tool. The Mosaic tool performs tile stitching automatically. Refer to Table 3.2 for the tiles' identification labels, and Figure 3.1 for tile cover overview.

Table 3.1: NAIP imagery characteristics, acquired through USGS EE.

Acquisition Date	Channels	Resolution	Flight Altitude	Sensor
June 28, 2014	R, G, B, NIR	1 m	17,500 ft 28,000 ft	Leica ADS 40
July 6-7, 2018	R, G, B, NIR	0.6 m	16,000 ft	Leica ADS 100

Table 3.2: NAIP tile Identification

NAIP 2014	NAIP 2018
m_4208233_nw_17_1_20140628	m_4208233_nw_17_060_20180706
m_4208233_se_17_1_20140628	m_4208233_se_17_060_20180706
m_4208233_sw_17_1_20140628	m_4208233_sw_17_060_20180706
m_4208241_ne_17_1_20140628	m_4208241_ne_17_060_20180706
m_4208241_nw_17_1_20140628	m_4208241_nw_17_060_20180706
m_4208338_ne_17_1_20140628	m_4208338_ne_17_060_20180707
m_4208338_se_17_1_20140628	m_4208338_se_17_060_20180707
m_4208339_ne_17_1_20140628	m_4208339_ne_17_060_20180706
m_4208339_nw_17_1_20140628	m_4208339_nw_17_060_20180707
m_4208339_se_17_1_20140628	m_4208339_se_17_060_20180706
m_4208339_sw_17_1_20140628	m_4208339_sw_17_060_20180707
m_4208340_ne_17_1_20140628	m_4208340_ne_17_060_20180706
m_4208340_nw_17_1_20140628	m_4208340_nw_17_060_20180706
m_4208340_se_17_1_20140628	m_4208340_se_17_060_20180706
m_4208340_sw_17_1_20140628	m_4208340_sw_17_060_20180706
m_4208346_ne_17_1_20140628	m_4208346_ne_17_060_20180707
m_4208347_ne_17_1_20140628	m_4208347_ne_17_060_20180706
m_4208347_nw_17_1_20140628	m_4208347_nw_17_060_20180707
m_4208347_se_17_1_20140628	m_4208347_se_17_060_20180706
m_4208348_ne_17_1_20140628	m_4208348_ne_17_060_20180706
m_4208348_nw_17_1_20140628	m_4208348_nw_17_060_20180706
m_4208348_sw_17_1_20140628	m_4208348_sw_17_060_20180706

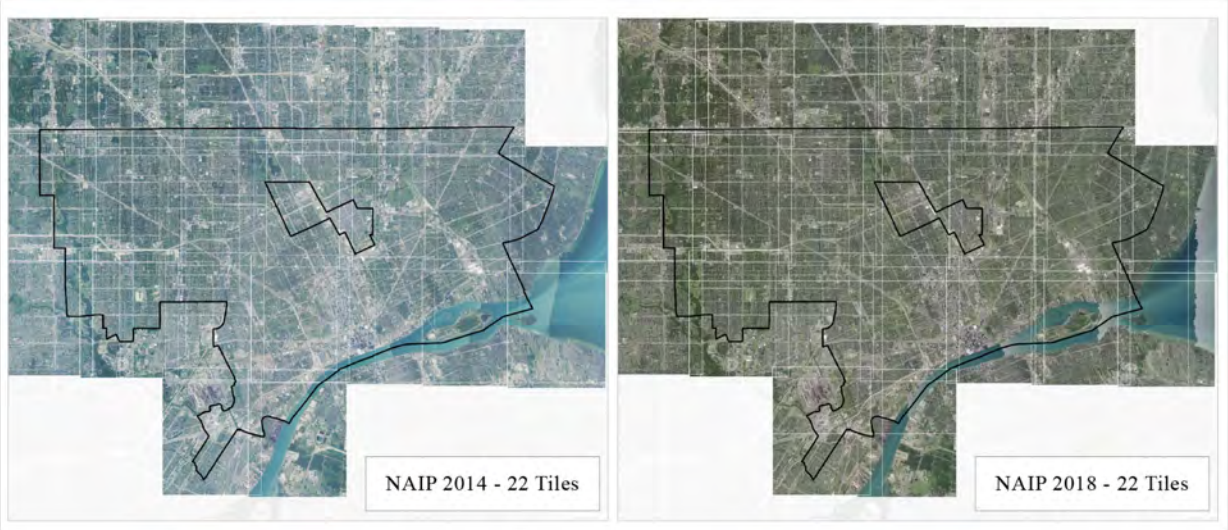

Figure 3.1: NAIP coverage of Detroit

3.1.1 Pre-Processing

Due to the strong vegetative vigour present in NAIP imagery, a NDVI was calculated based on 32-bit real values. NDVI is the most common index for assessment of vegetation, as it quickly delineates vegetation (Huang *et al*., 2020), and therefore was applied in this analysis. Due to differences in spatial resolution between the two imagery datasets, resampling was conducted to match pixel registration and spatial resolution. This step is needed to ensure consistency when comparing total class's land cover areas. Based on the area of interest, the NAIP 2014 imagery was resampled to 0.6m with the Nearest Neighbour method (Figure 3.2).

Figure 3.2: NAIP 2014 resampling from 1m to 0.6 m with Nearest Neighbour method

3.2 Ancillary Vector Data

In addition to raster data, the study used various vector files acquired from the City of Detroit Open Data Portal and Data Driven Detroit (Table 3.3). To classify residential structure change between NAIP 2014 and NAIP 2018, parcel lot vector data was used as the classification boundary and downloaded from the City of Detroit Open Data Portal (City of Detroit, 2021b). To

select areas of interest representing a variety of changes which occurred between the two NAIP imagery sets, three residential demolition rates are calculated based on administrative neighbourhood boundaries (City of Detroit, 2021c). For reference and validation, Complete Residential Demolitions (City of Detroit, 2021a), and Motor City Mapping (Data Driven Detroit, 2014a) vector files were used.

Table 3.3: Vector Data

File Name	Source
Parcels	City of Detroit Open Data Portal
Current City of Detroit Neighbourhoods	City of Detroit Open Data Portal
Completed Residential Demolitions	City of Detroit Open Data Portal
Motor City Mapping, Winter 2013-14 Certified Results	Data Driven Detroit

CHAPTER 4: Methodology

4.1 Developing Classification Workflow and Model

Image analysis was performed using CATALYST Professional Focus software, and their Object Analyst tool. Parcel classification and change detection was conducted using ArcGIS Pro.

A pilot study area was used to identify appropriate image segmentation parameters, classification features, and to generate a classification model. Those findings were later applied to three neighbourhoods in Detroit. Due to computational demands, a 2.59 square kilometre (one square mile) extent within Detroit was selected to represent urban residential ground conditions on which testing was performed (Figure 4.1). The parameters were tested on the NAIP 2018 imagery set due to its original higher resolution than NAIP 2014 data. Once the workflow was established to be appropriate for the 0.6m NAIP 2018 imagery, it was applied to NAIP 2014 imagery and evaluated to determine whether the same parameters required adjustment. It is not obvious that imagery with different spatial resolutions, sensors, and flight altitudes would perform similarly with identical parameters. It was important to identify a segmentation that would produce image-objects resistant to shadow impacts, since the two imagery sets have opposing shadow directions (Figure 4.2). Various researchers (both pixel and object-based) describe shadows as a challenge for analysis (Hussain *et al.*, 2013; Toney *et al*., 2012). For instance, features such as water, shadows, roads, and building rooftops may have similar spectral values (Hossain and Chen, 2019). The final classification is composed of two classes: *Impervious* and *Pervious*. One aim of the segmentation and classification is the delineation of surfaces under shadows. Additional classes introduce complexity, especially when selecting appropriate ground features representing samples for classes. For this study, *Pervious* represents all types of vegetation (trees, bushes, lawns, grass, and other green biomass). *Impervious* represents the opposite of vegetation, including roads,

asphalt, cars, bare soil, and rooftops. Water was included in this class to distinguish it from vegetation.

Figure 4.1: 2.59 square kilometre (one square mile) extent, NAIP 2018

Figure 4.2: NAIP imagery, opposing direction of shadows

4.1.1 Image Segmentation

A multiresolution segmentation was performed, based on the availability of parameters within CATALYSTs Object Analyst tool (Figure 4.3). Previous studies adopted an experimental approach when deciding on the optimal segmentation parameters (Ellis and Mathews, 2019; Jayasekare *et al*., 2017; Norman *et al.*, 2021; Shahi *et al*., 2016; Yen *et al*., 2020). In this study,

the parameter values were identified in the following order: shape and compactness, image channels, and lastly, scale. Despite descriptions of scale as the most important parameter (Maxwell *et al.*, 2019), scale is supplementary to the shape and compactness parameters in this study. This is due to the underlying emphasis the shape and compactness have on the boundaries of the image-objects generated. In the Object Analyst tool, the options for the shape and compactness range between 0.1-0.9, where 0.1 indicates a low weight and 0.9 the highest. To understand the impact of various weight combinations, an experimental approach was applied, and three values were chosen to represent low (0.1), medium (0.5) and high (0.9) shape and compactness. Those were segmented based on the Red, Green, Blue (RGB) bands with a scale of 5, and crossed with each other, resulting in a 3x3 matrix (Figure 4.4). Based on a visual interpretation, the best performing shape and compactness were chosen. Once the shape, compactness and bands were established, a series of various scales was performed in increments of 10 (5, 15, 25).

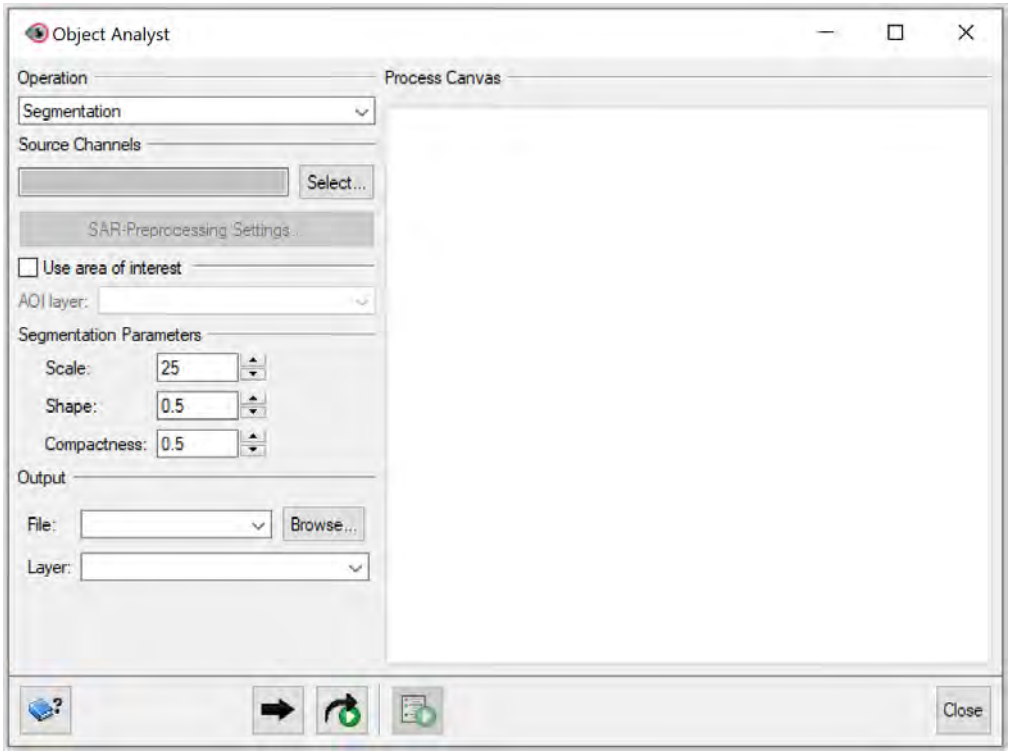

Figure 4.3: CATALYST Object Analyst - segmentation parameters

Figure 4.4: Image segmentation shape and compactness matrix example. Based on the RGB bands, with a scale of 5.

4.1.2 Training Model and Validation

The literature does not describe in exact terms recommendations for training objects. Maxwell *et al*. (2019) suggests that training and validating objects should be many. In this study, 75 designated areas per class (a total of 150 areas) were chosen as a selection of surfaces for training and validation objects. These areas represent a variety of pervious and impervious

surfaces. Within each area, two objects were selected for the training model, and two validation objects for future classification accuracy (Figure 4.5). Near-identical objects were selected for training and validating. The identification of ground features was performed by visual interpretation with the help of false infrared channel combination. Close attention was paid to selecting similar ground features obscured by shadows to maintain consistency and breadth of variety for training/validating objects. In instances where the generated boundary included both pervious and impervious surfaces, the object was assigned based on the majority of surface covered. If an object contained 50/50, it was not used for training or validation. This was intended to ensure that objects representing *Pervious* and *Impervious* surfaces are as true to reality as possible.

Figure 4.5: Training/validating image-objects areas and examples

4.1.3 Classification

Object Analyst supports two machine learning classifiers: Random trees (RT), and Support Vector Machine (SVM). In this study, the SVM classifier method was used with a Radial Basis Function and Normalized data, based on the default settings within Object Analyst. For the classification, only statistical features were used. Since the objective was not to generate real-life objects, but rather differentiate between pervious and impervious surfaces, geometrical attributes were excluded, and only statistical features were tested. To identify the combination of statistical features that would yield the highest accuracy, a set of 12 experimental classifications were performed (Table 4.1). This systematic approach was developed for this analysis, based on the available statistical values within Object Analyst tool. The first four sets of classifications tested the accuracy of RGB channels, the second four classifications included NIR, and the last set of four classifications introduced the NDVI values. Statistical values calculated for each image-object were minimum, maximum, mean, and standard deviation. The advantage of performing the classifications systematically is to identify if a pattern emerges based on a certain set of statistical combinations.

Table 4.1: Statistical attribute selection

Channels Used	RGB	RGB, NIR	RGB, NIR, NDVI
Statistical Attributes	1. Min, Max, Mean, Std. 2. Min, Max, Mean 3. Mean 4. Min, Max, Std.	5. Min, Max, Mean, Std. 6. Min, Max, Mean 7. Mean 8. Min, Max, Std.	9. Min, Max, Mean, Std. 10. Min, Max, Mean 11. Mean 12. Min, Max, Std.

4.1.4 Classification Accuracy Assessment.

Researchers working with GEOBIA methods indicate that there is insufficient research attention with respect to accuracy assessment (Johnson and Ma, 2020). One of the challenges in assessing the accuracy of image-objects based on a single pixel method is that the classification results can be misrepresented. For this study, an Overall Statistics and Error Matrix were used to assess an object's classification accuracy. The reason for this is threefold: (a) there is no clear consensus of a method to be used, (b) previous GEOBIA research has used the Confusion/Error Matrix (Norman *et al*., 2021), and (c) within Object Analyst the Accuracy Statistics and Error Matrix are built in as default.

4.1.5 Batch Application

VHR imagery requires high computational power to process large areas. Due to high volumes of data, the developed model was applied to other areas of Detroit for validation of performance and visual inspection to ensure it performed similarly in other areas of the city.

To perform batch classification and rule out the need to create a new model for NAIP 2014 imagery, the model developed for NAIP 2018 was applied to the NAIP 2014 (resampled to 0.6m) imagery. If the training model developed for NAIP 2018 was successful in detecting Pervious/Impervious surfaces, it would be used as the training model for classification of NAIP 2014. If unsuccessful, a new set of image-objects would be selected based on the designated training areas for NAIP 2014.

4.2 Parcel Classification and Change Detection

Thompson and de Beurs (2018) classified parcel lots into structure/no structure classes based on remotely sensed data and classifies parcel lots based on structure presence. The parcel lot status for this study was established by the total *Impervious* land cover area of each residential parcel lot. To classify the parcel lots, a series of queries evaluating thresholds were performed. To validate the accuracy of the thresholds, the parcel lots within the study area were manually classified.

4.2.1 Parcel Status Validation

Initially, the validation was meant to be conducted based solely on the ancillary vector data. However, a substantial number of records did not accurately represent ground conditions. For instance, certain residential demolitions were not recorded in the Complete Residential Demolitions shapefile but based on visual comparison of the two imagery sets, a structure had clearly been demolished. Additionally, when comparing the Motor City Mapping file, the structure/no-structure field did not always correspond to present ground features in the 2014 imagery set. Based on that, each parcel's status was assigned manually, with the help of vector data from the Detroit Open Data Portal and Data Driven Detroit as well as the NAIP imagery, for confirmation when visual interpretation proved difficult. To help interpret ground features accurately the following methods were incorporated: (a) multitemporal observation – observing for clues from different times. (b) False colour infrared imagery – helping with impervious surfaces hidden under shadows. (c) Cross referencing with ancillary vector shapefiles, such as Complete Residential Demolitions and Motor City Mapping. Parcels were assigned with a numerical value, where one represents an absence of residential structure, and two represents the presence of

residential structure. This step was applied to the 2.59 square kilometre (one square mile) tile and the three neighbourhoods of interest for the NAIP 2014 and NAIP 2018 data sets. In total, 19,532 parcel lots were visually interpreted and manually classified as validating features. Parcel change between NAIP 2014 and NAIP 2018 was classified into four classes of change: *Structure Remained, Structure Demolished, Remained Empty,* and *New Structure.* Visual inspection was performed on all types of parcel lots within the areas of interest. However, the demolition change detection analysis was performed on parcel lots zoned as Residential.

4.2.2 Thresholds Classifying Residential Parcel Lots and Change Detection

Based on the known residential lot vacancy, a mean *Impervious* land surface square metre area was calculated and used as a threshold for queries. Based on visual interpretation of the imagery, there were 1,060 vacant residential parcel lots out of a total 2,292 residential parcel lots in NAIP 2018 imagery. The mean *Impervious* land cover on those parcel lots was 19.7 square metres. Therefore, the first threshold assumes a residential structure is present on a residential lot if the *Impervious* land area surface classified is above 20 square metres. Increments of +5 square metre of *Impervious* land surface were tested up to 30 square metres. Accuracy was assessed and validated based on the visual interpretation of the parcels. Subsequently, a single threshold of 25 square metres was selected and change detection of residential parcel lots was performed. Demolition rate accuracy calculations were as follows:

$$\text{Selected} = [\text{Selected Residential Demolitions}/\text{Total Number of Residential Demolitions}]*100 \quad (1)$$

$$\text{Error (of Commission)} = [\text{Incorrectly Detected} / \text{Total Selected}]*100 \quad (2)$$

4.3 Application on Three Areas

Once the classification model and best threshold to classify Parcel Lots were established, identical GEOBIA parameters were applied to three neighbourhoods of interest in Detroit, representing high, median, and low residential demolition rates between 2014-2018 (Table 4.2). Residential demolitions do not occur uniformly across space, and it is important to validate the performance of the workflow across different rates of change. The aim was to assess different changes in ground conditions, and whether the workflow performs similarly across a variety of urban environments. To calculate the residential demolition rates between the two NAIP imagery sets, the residential demolitions were selected between June 30, 2014, and July 6, 2018, totaling 13,657 residential demolitions city wide. This number is calculated into a rate, based on the neighbourhood's administrative boundaries, and the total of residential parcel lots present within. To ensure a sufficient sample number, the neighbourhoods had to have at least 1,000 residential parcel lots. The first neighbourhood was Crary/St Mary, representing a low residential demolition rate of 0.83%. The second neighbourhood was Core City, containing the median residential demolition rate of 2.9%. The third neighbourhood was Pulaski, representing a very high residential demolition rate of 12.1%. (Figure 4.6).

Table 4.2: Three chosen neighbourhoods, residential demolition rates based on Complete Residential Demolitions, City of Detroit Open Data Portal (2021a)

Neighborhood	Residential Parcel Lots	Residential Demolitions 2014-2018	Residential Demolition Rate	
Crary/St. Mary (low)	3,226	27	0.83%	
Core City (median)	1,161	34	2.9%	
Pulaski (high)	2,403	291	12.1%	

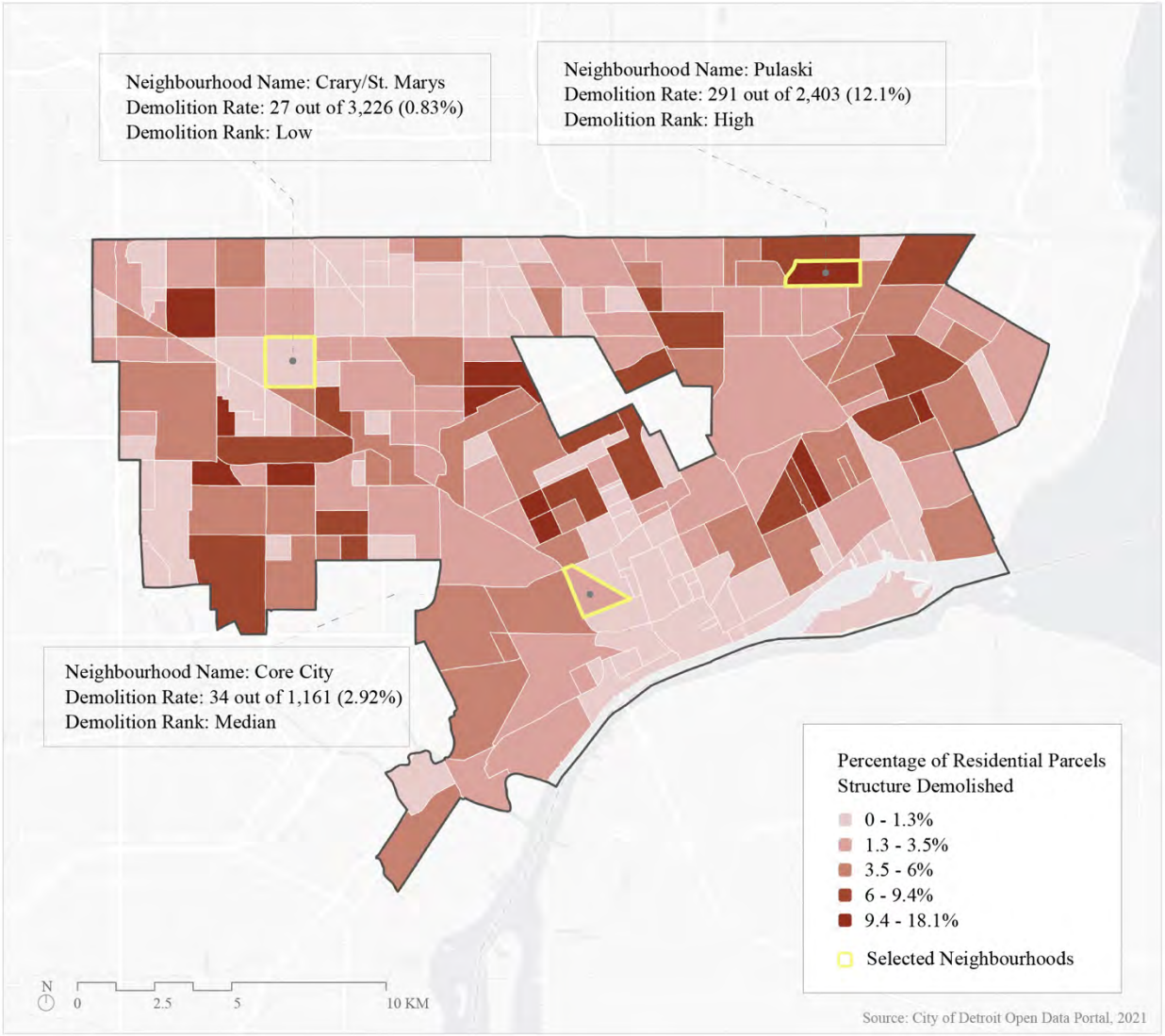

Figure 4.6: Residential demolition rates by neighbourhood, and three areas of interest, between 2014-2018 NAIP imagery

CHAPTER 5: Results and Discussion

5.1 GEOBIA Workflow Repeatability

5.1.1 Image Segmentation, Feature Selection, and Classification Accuracy

Based on experimentation, the most suitable parameter combination to generate image-objects least effected by shadows was segmentation on the Blue and NDVI channels with a scale of 5, shape of 0.1, and compactness of 0.9 (Figure 5.1). Within the 2.59 square kilometre (one square mile) extent, this combination generated 165,320 image-objects in NAIP 2014 and 263,639 image-objects in NAIP 2018 image (Table 5.1). The vast difference in number of objects can be attributed to the initial resolution difference. Since the NAIP 2014 imagery has a slightly lower resolution than the NAIP 2018 imagery, fewer ground features were registered in the image, resulting in a more 'foggy' or 'blurry' appearance. Despite the apparent over-segmentation of real-life objects, the segmentation was successful at delineating pervious and impervious surfaces under shadows and was therefore suitable for this analysis.

Figure 5.1: Tile extent - image segmentation outcomes in 2014 and 2018 based on Blue and NDVI channels, scale of 5, shape of 0.1, and compactness of 0.9

Table 5.1: Image-objects and class objects

Imagery	Total Image-Objects	*Pervious* Objects	*Impervious* Objects
2014	165,320	1,360	1,498
2018	263,639	2,388	8,161

In the feature selection step, the best classification accuracy was achieved when all channels and the NDVI were used, with statistical values of mean only (Table 5.2). Other statistical combinations also performed with similarly high accuracy values. For instance, the inclusion of all available statistical measures among the visible spectrum resulted in 98% overall accuracy, suggesting that it is possible to achieve meaningful results with visible light only. Based on the following 12 classifications, when features included only mean statistical values, the classification performed either the best, or second best. This indicates that additional statistical features such as maximum, minimum, and standard deviation do not necessarily increase the classification accuracy in this context.

Table 5.2: NAIP 2018, statistical features, classification accuracies

Attribute Channels	Statistical Features				Overall Accuracy
	Min	Max	Mean	Std.	
RGB	+	+	+	+	98%
RGB	+	+	+		97.6%
RGB			+		97.6%
RGB	+	+		+	96.3%
RGB, NIR	+	+	+	+	97.6%
RGB, NIR	+	+	+		98.0%
RGB, NIR			+		98.0%
RGB, NIR	+	+		+	96.6%
RGB, NIR, NDVI	+	+	+	+	97.0%
RGB, NIR, NDVI	+	+	+		97.3%
RGB, NIR, NDVI			+		98.3%
RGB, NIR, NDVI	+	+		+	95.3%

The first classification was performed on the NAIP 2018 imagery 2.59 square kilometre (one square mile) extent, yielding an overall accuracy of 98.3%. In NAIP 2018, the *Pervious* class

covered 1.77 square kilometres and the *Impervious* class covered 0.81 square kilometres. Refer to Table 5.3 for full accuracy statistics, Table 5.4 for the error matrix, and Figure 5.2 for the tile overview.

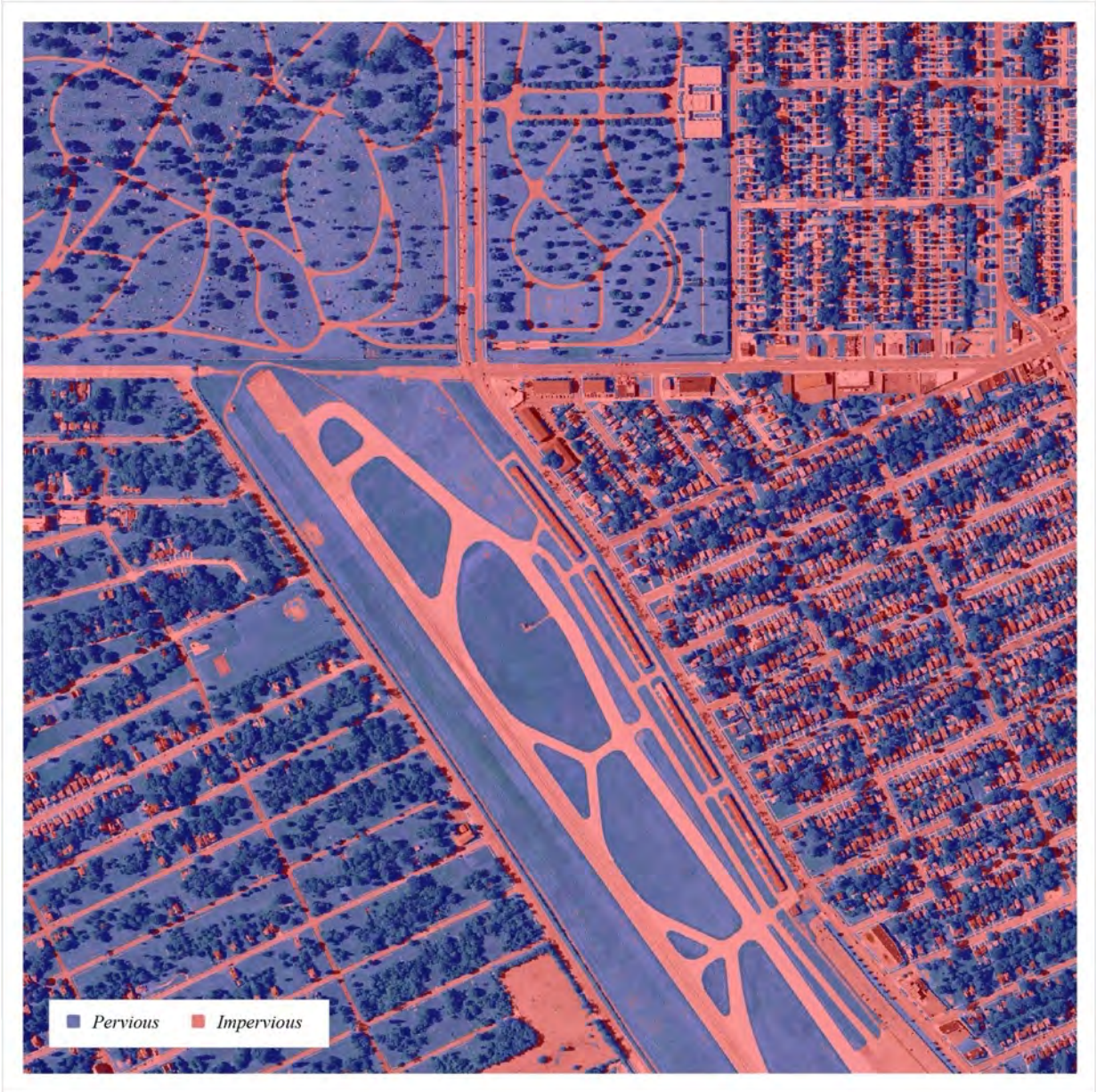

Figure 5.2: NAIP 2018 2.59 square kilometre (one square mile) tile extent - classification result

Table 5.3: 2018 Accuracy Statistics Report of 300 sampling objects

Class Name	**Producer's Accuracy**	**95% Confidence Interval**	**User's Accuracy**	**95% Confidence Interval**	**Kappa Statistic**
Pervious	99.333%	(97.697% 100%)	97.385%	(94.530% 100%)	0.947
Impervious	97.333%	(94.421% 100%)	99.319%	(97.650% 100%)	0.986
Overall Accuracy: 98.333%			95% Confidence Interval (96.717% 99.948%)		
Overall Kappa Statistic: 0.966			Overall Kappa Variance: 0.666		

Table 5.4: 2018 Error (confusion) Matrix

Classified Data	**Reference Data**		
	Pervious	*Impervious*	**Totals**
Pervious	149	4	153
Impervious	1	146	147
Totals	150	150	300

Based on the object classification conducted on the NAIP 2018 image, the training model was applied to NAIP 2014 image. However, the training model did not perform successfully and classified all but six image-objects into the *Pervious* class. This may be due to the radiometric difference between the two imagery datasets because of different sensors, and the reflectance of the red and NIR channels could be different between those two dates (since those bands are responsible for the NDVI, and the NDVI is a major component of the classification). Based on the designated areas developed earlier in the study, the training objects had to be re-selected for the NAIP 2014 imagery. Attention was paid to selecting the most similar objects as possible to ensure consistency between the two sets of imagery. Once the training objects were assigned, the classification was performed again. Image segmentation parameters, attribute features, and the SVM classifier remained the same, and the only difference was the objects of the training model. The classification resulted in an identical overall accuracy of 98.33%, suggesting that the choice of objects for training was successful. In NAIP 2014, the *Pervious* class covered 1.74 square

kilometres and the *Impervious* class covered 0.84 square kilometres. Refer to Table 5.5 for full accuracy statistics, Table 5.6 for the error matrix, and Figure 5.3 for the tile overview.

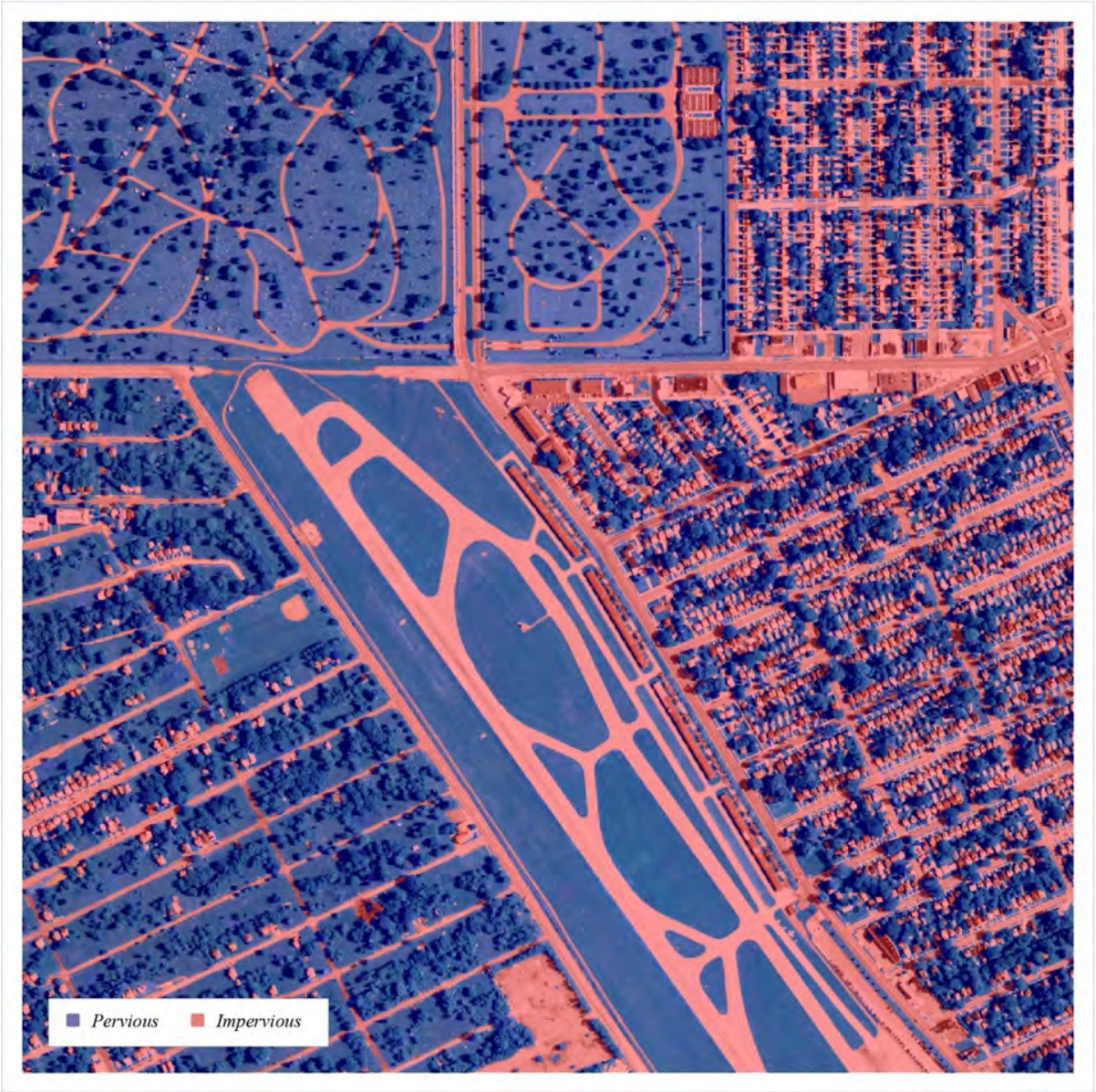

Figure 5.3: NAIP 2014 2.59 square kilometre (one square mile) tile extent - classification result

Table 5.5: 2014 Accuracy Statistics Report of 300 sampling objects

Class Name	**Producer's Accuracy**	**95% Confidence Interval**	**User's Accuracy**	**95% Confidence Interval**	**Kappa Statistic**
Pervious	100%	(99.666% 100%)	96.774%	(93.670% 99.878%)	0.935
Impervious	96.666%	(93.460% 99.872%)	100%	(99.655% 100%)	1
Overall Accuracy: 98.333%			95% Confidence Interval (96.717% 99.948%)		
Overall Kappa Statistic: 0.966			Overall Kappa Variance: 0.000		

Table 5.6: 2014 Error (confusion) Matrix

Classified Data	**Reference Data**		
	Pervious	*Impervious*	**Totals**
Pervious	150	5	155
Impervious	0	145	145
Totals	150	150	300

5.1.2 Batch Classification and Application to Areas of Interest

When the GEOBIA training model was applied to the three areas of interest, it performed similarly based on visual inspection (Figures 5.4 - 5.6). This suggests that the same parameters and training model can be applied to other areas that were acquired on the same date, with the same sensor, and the same flight altitude. However, the image classification did not perform flawlessly. For instance, rooftops present in the Crary/St. Mary area of interest were more susceptible to error due to shadows. The introduction of radiometric differences during NAIP image pre-processing might explain this phenomenon.

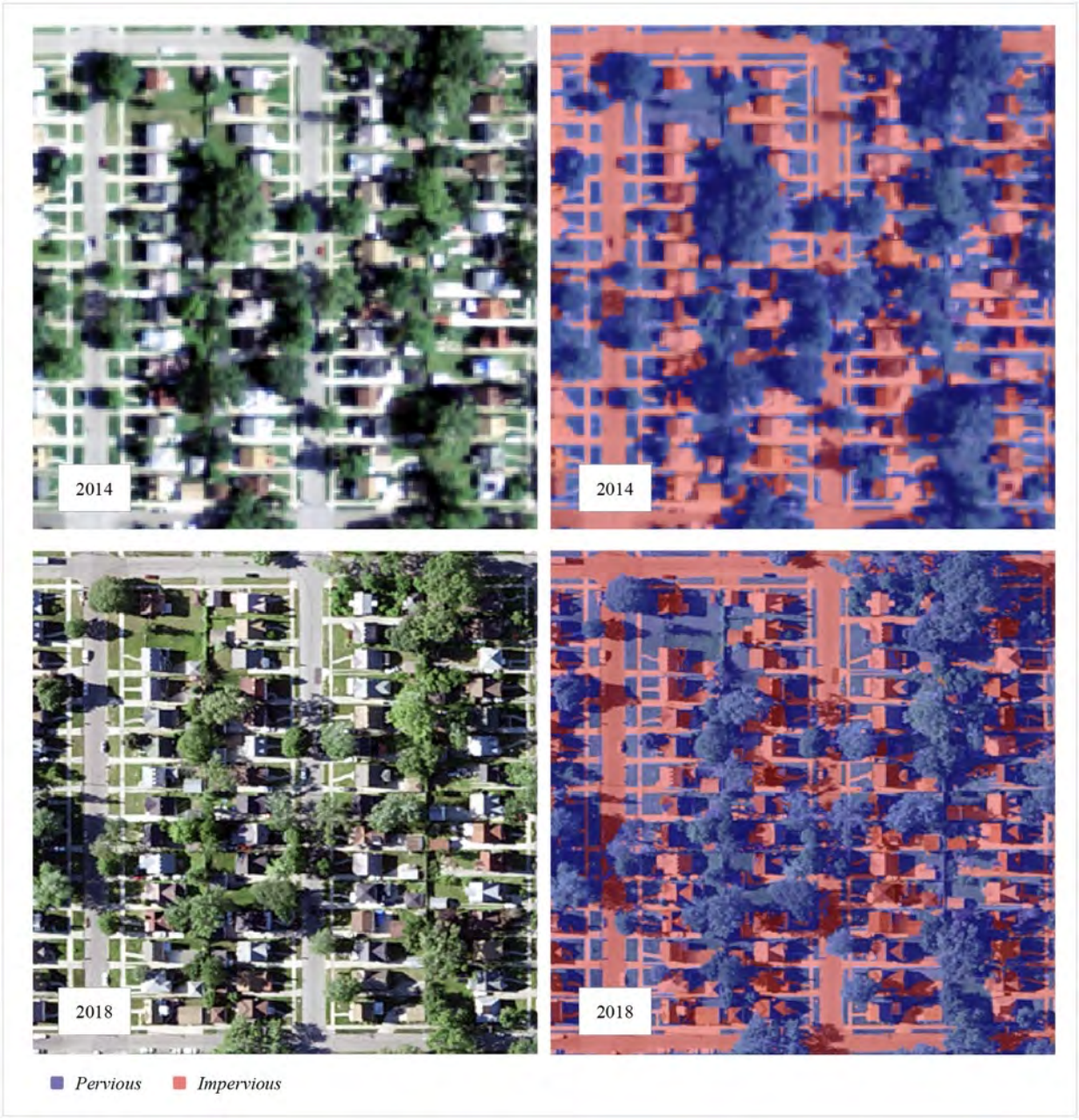

Figure 5.4: Batch GEOBIA, low demolition rate, Crary/St. Mary, Detroit

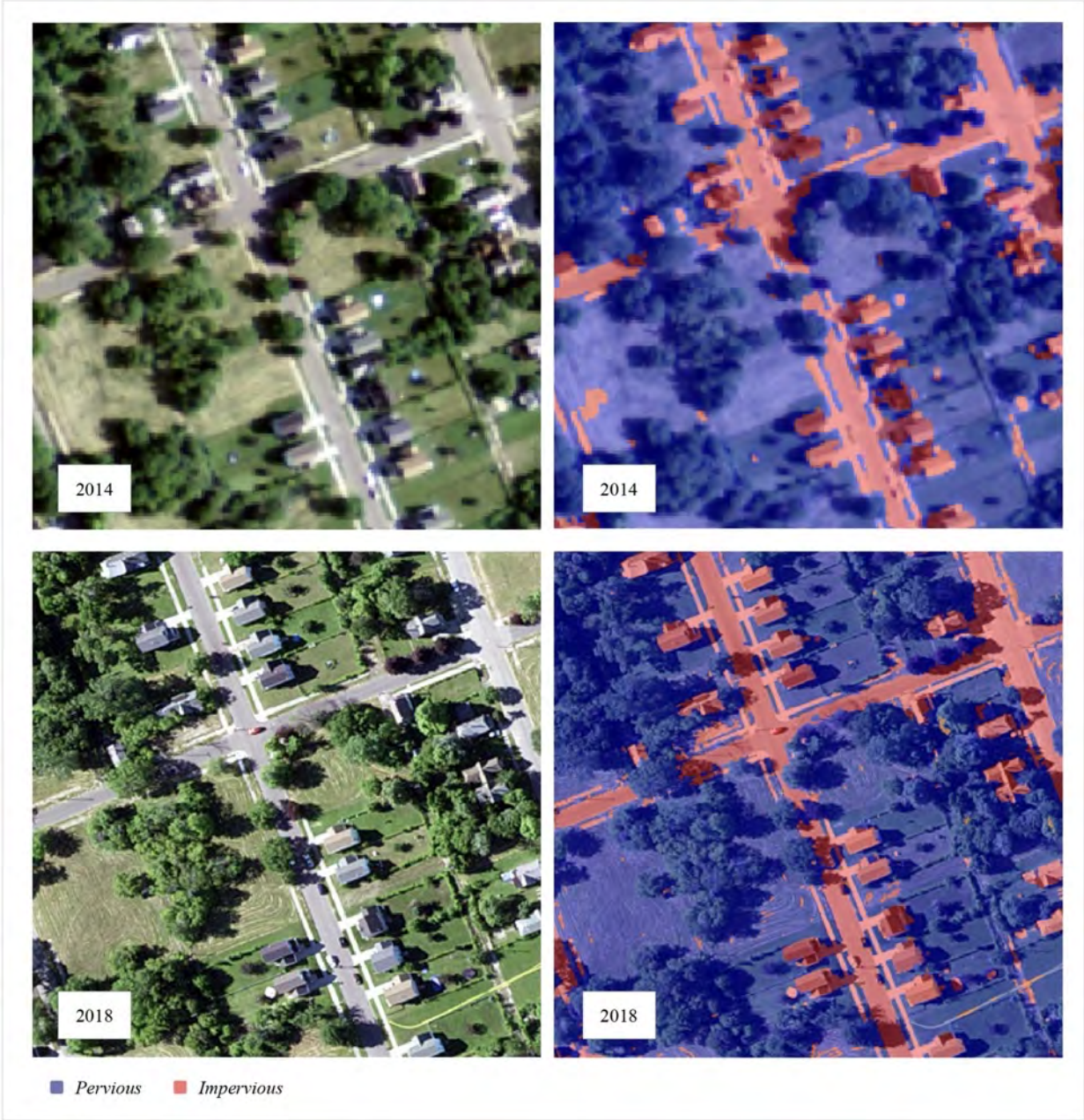

Figure 5.5: Batch GEOBIA, median demolition rate, Core City, Detroit

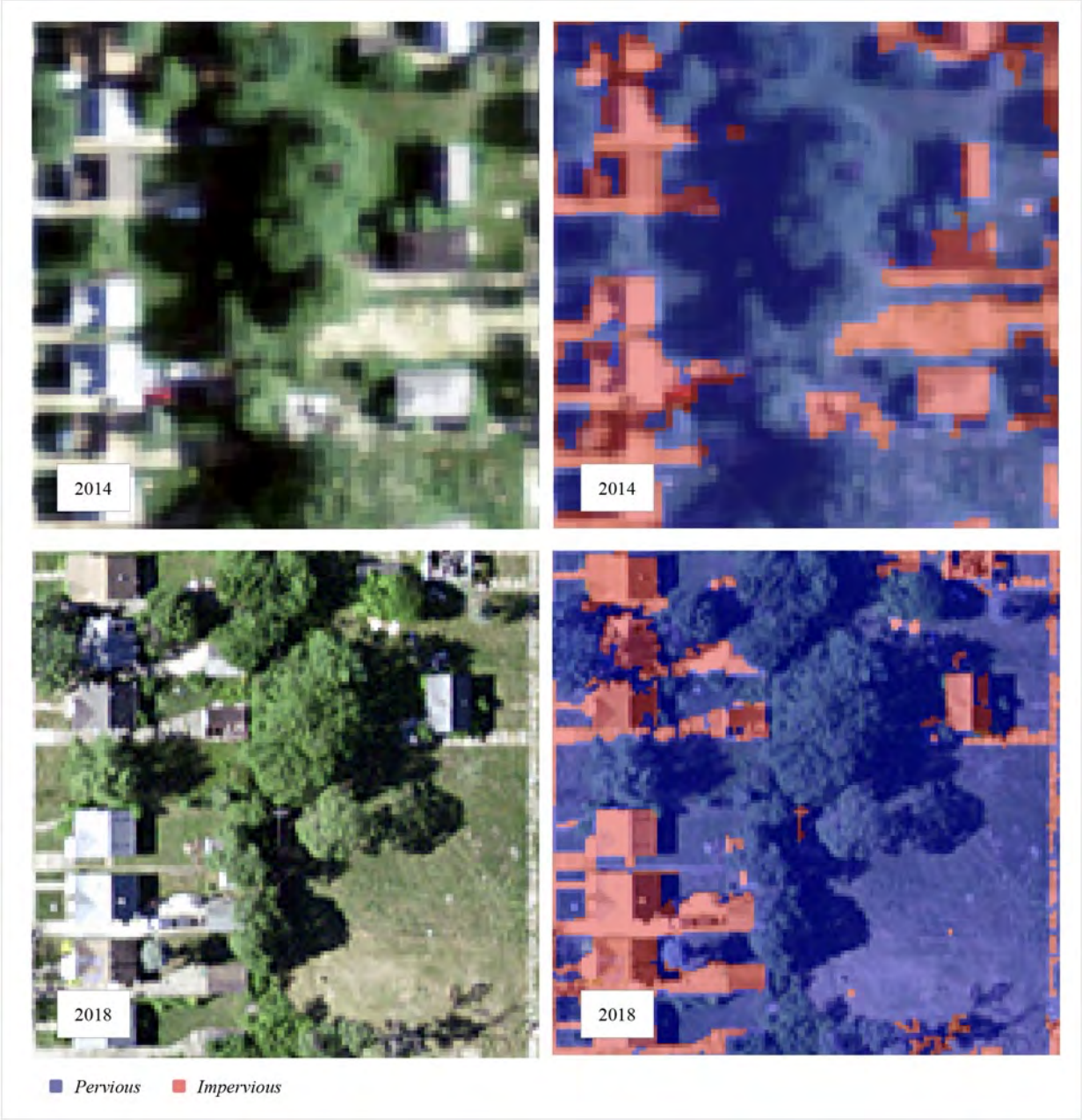

Figure 5.6: Batch GEOBIA, high demolition rate, Pulaski, Detroit

5.2 Parcel Classification and Change Detection

Impervious surfaces were clipped to parcels contained within the 2.59 square kilometre (one square mile) tile extent. Figure 5.7 illustrates the NAIP 2014 tile extent and Figure 5.8 illustrates the NAIP 2018 extent. When layers are overlapped, NAIP 2014 is larger than the

boundaries generated based on NAIP 2018 (Figure 5.9). Despite the opposing shadow directions, both classifications were able to generate very similar boundaries.

Figure 5.7: NAIP 2014 *Impervious* surfaces on parcel lots

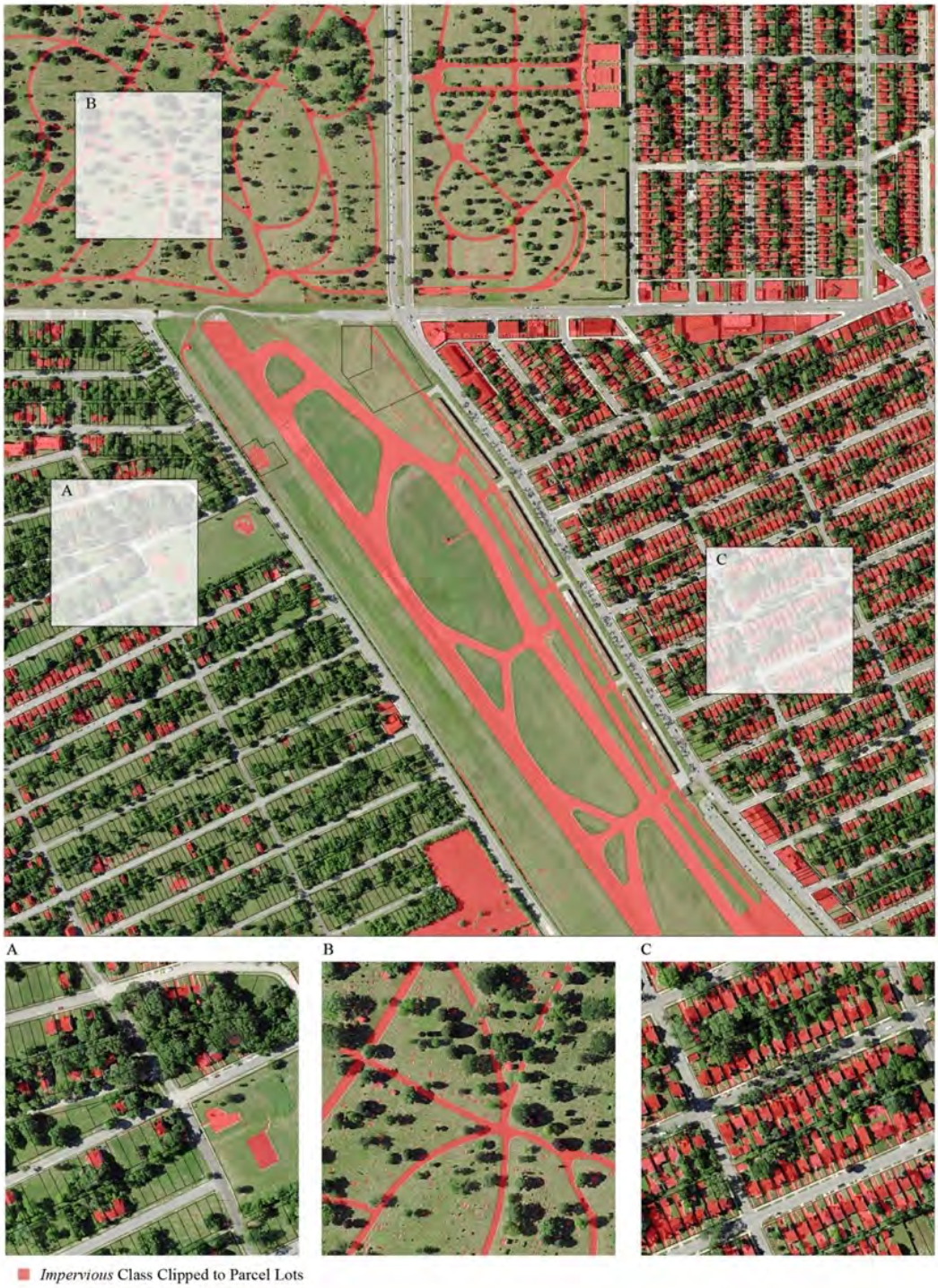

Figure 5.8: NAIP 2018 *Impervious* surfaces on parcel lots

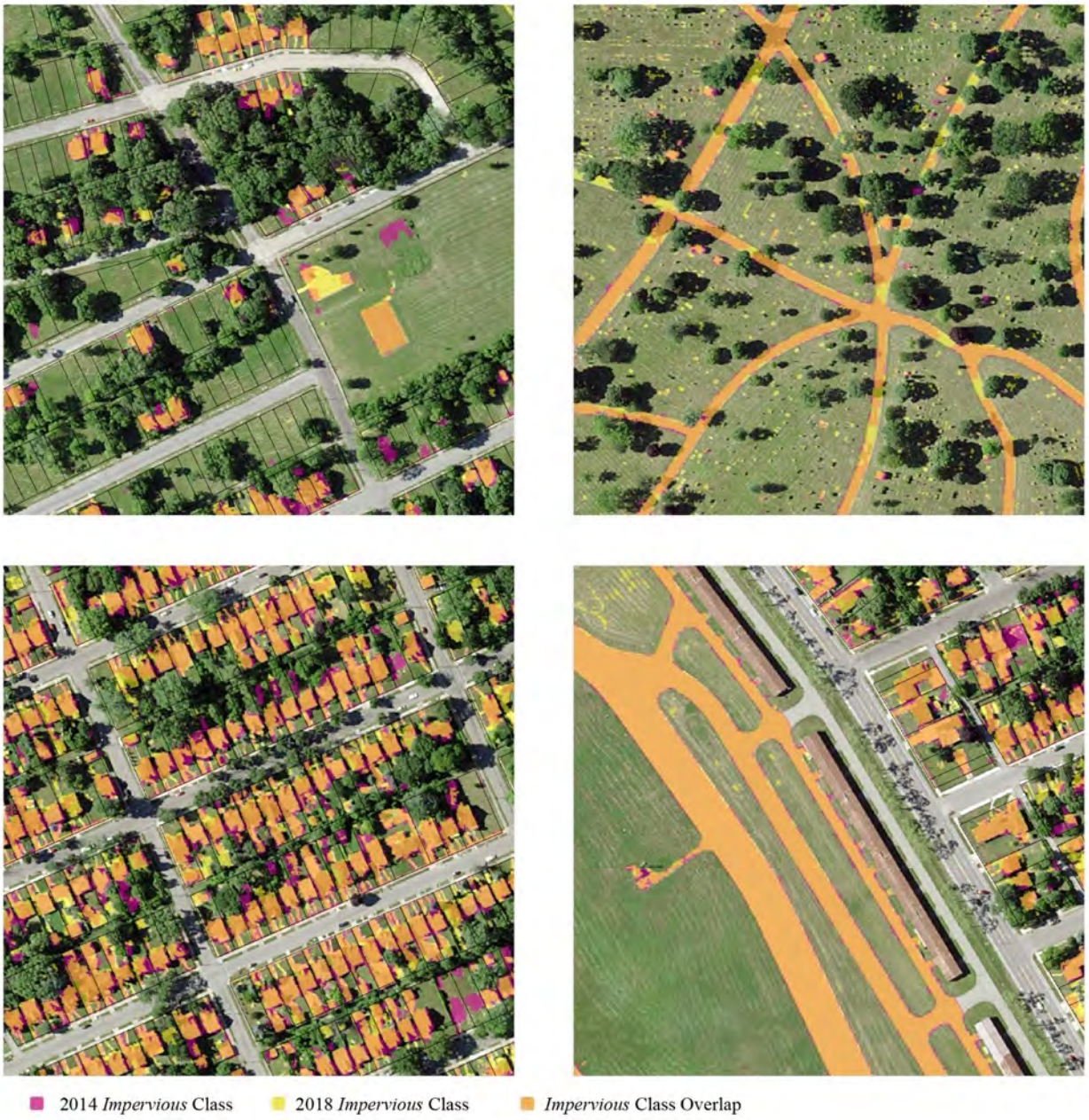

Figure 5.9: *Impervious* surface overlap on parcel lots

5.2.1 Visual Interpretation and Change Detection From-To

Four classes represent the change captured between the NAIP 2014 and 2018 imagery sets: (a) *Structure Remained* – Parcel lot contained a structure in both data sets, (b) *Structure Demolished* – A structure existed in NAIP 2014, but an empty parcel lot in 2018, (c) *Remained*

Empty – Parcel lot is vacant in both imagery sets, (d) *New Structure* – Parcel lot did not contain a structure in 2014 and did contain a structure in 2018. According to the visual inspection of the NAIP imagery datasets, within the 2.59 square kilometre (one square mile) tile extent, 66 (2.78%) demolitions occurred (Figure 5.10). In Crary/St. Mary (low rate), 32 (0.94%) occurred. In Core City (median rate), 35 (2.37%) occurred. In Pulaski (high rate), 295 (11.61%) occurred. Table 5.7 describes the number of parcel lots within each class, and Figure 5.11 maps the three areas of interest.

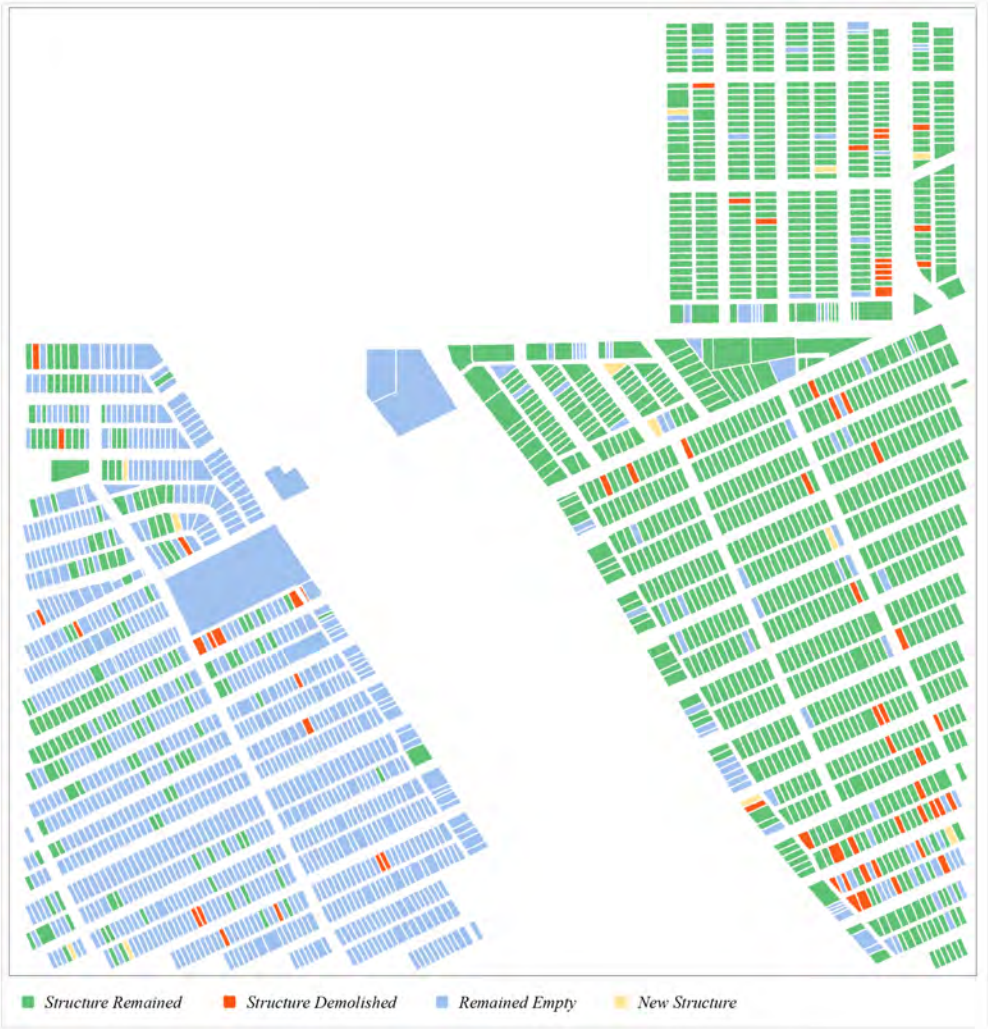

Figure 5.10: 2.59 square kilometre (one square mile) tile extent – visually observed change detection: NAIP 2014- NAIP 2018

Figure 5.11: Three areas of interest, visually observed change detection: NAIP 2014 – NAIP 2018

Table 5.7: Visual change detection

Aera of Interest	**Total Parcel Lots**	**Residential Parcel Lots**	***Structure Remained***	***Structure Demolished***	***Remained Empty***	***New Structure***
Tile Extent	2,370	2,292	1,267	66	1,025	12
Low (Crary/St. Mary)	3,380	3,226	3,194	32	152	2
Median (Core City)	1,476	1,161	364	35	1,023	13
High (Pulaski)	2,540	2,403	1,925	295	320	0

5.2.2 Detection of Structures and Parcel Classification Based on Thresholds

This analysis captures residential demolitions. Therefore, the queries performed include results based solely on residential parcels. Within the NAIP 2018 2.59 square kilometre (one square mile) tile extent, there are 1,060 empty residential parcel lots, in which the mean *Impervious* land surface area is 19.78 square metres. This figure guided the decision for a threshold for structure presence on a residential parcel lot. Increments of five square metres up to 30 were tested to attempt to capture more residential lots that were empty. The first query, which assumes a parcel lot is empty if the total area of *Impervious* is 20 square metres or less, detected 88.49% of the total empty residential parcel lots. When the threshold was increased, more empty parcels were detected. However, this also introduced more commission error (included in a class it does not belong too). The same methodology yielded similar results with consistently higher commission rates when applied to the 2014 NAIP tile extent. However, this did not hold true when similar thresholds were applied to the three neighborhoods of interest. While successful detection rates of residential parcels containing structures decreased to as low as 63%, the commission error in some instances reached as high as 82%. The fewer empty residential parcels, the worse the detection method performed. Refer to Table 5.8 for structure detection accuracies.

Table 5.8: Residential structure detection by parcel lot – accuracy comparison

Area of Interest	Observed Empty Residential Parcel Lots	Mean Empty Residential Parcel in Sq. Metres	No. of Residential Parcels Selected When *Impervious* area under x Sq. Metres:								
			20	Selected	Error	25	Selected	Error	30	Selected	Error
Tile Extent 2014	1,006	10.36	915	89.26%	1.85%	934	90.75%	2.24%	951	92.04%	2.62%
Tile Extent 2018	1,060	19.78	945	88.49%	0.74%	972	90.84%	0.92%	994	92.64%	1.20%
Low 2014	122	28.12	251	79.50%	61.35%	285	81.96%	72.90%	321	86.06%	82.07%
Low 2018	147	45.23	144	70.06%	28.47%	164	72.10%	35.36%	189	75.51%	41.26%
Median 2014	837	26.02	623	73.35%	1.44%	648	76.34%	1.38%	681	80.16%	1.46%
Median 2018	860	26.85	603	69.41%	0.99%	646	74.18%	1.23%	682	78.13%	1.46%
High 2014	266	43.56	325	65.78%	46.15%	366	68.79%	50.0%	396	71.42%	52.02%
High 2018	561	46.04	404	63.99%	11.13%	440	66.31%	14.09%	475	71.12%	16%

Within the select square metre thresholds, NAIP 2018 consistently detected fewer vacant residential parcel lots than NAIP 2014. Conversely, the commission error in NAIP 2014 was consistently larger than in NAIP 2018. With the same land area, more residential lots were selected, increasing both the rate selection as well as the inclusion of falsely identified empty lots. This may be due to the different original imagery spatial resolutions and different conditions and view angles of vegetation surrounding rooftops.

5.2.3 Change Detection Between NAIP 2014-2018

The 25 square metre threshold was investigated for residential parcel lot change detection between the two imagery sets. Here, they are compared to the visually observed residential parcel lot demolitions (Table 5.9). The highest rate of successfully detected demolitions is 57.57% and is within the 2.59 square kilometre (one square mile) tile extent. However, 53.08% of the total selection was falsely detected. Table 5.10 describes the classes to which the selected parcels belonged. Figures 5.12 – 5.15 map the undetected residential parcel lots that were demolished between NAIP 2014 and NAIP 2018, the successfully detected demolitions, and the residential parcel lots that were selected but did not experience demolition between the two dates. The average successful detection rate was 42% and the average commission error was 62%.

Table 5.9: Change detection of residential parcel lots based on 25 square metre threshold

Area of Interest	Observed Demolitions	No. of Parcels Selected at 25 Sq. m. of Impervious	Successfully Selected out of Total Demolitions	Commission Error
Tile Extent	66	81	57.57%	53.08%
Low	27	33	29.62%	75.75%
Median	32	104	37.5%	88.46%
High	295	196	44.06%	33.67%
Average:			42.18%	62.74%

Table 5.10: 25 square metre of *Impervious* land areas as structure threshold selection breakdown

Observed Parcel Lot Condition	Tile Extent	Low	Median	High
Remained Empty	37	7	86	40
Structure Demolished	38	8	12	130
Structure Remained	6	18	6	26

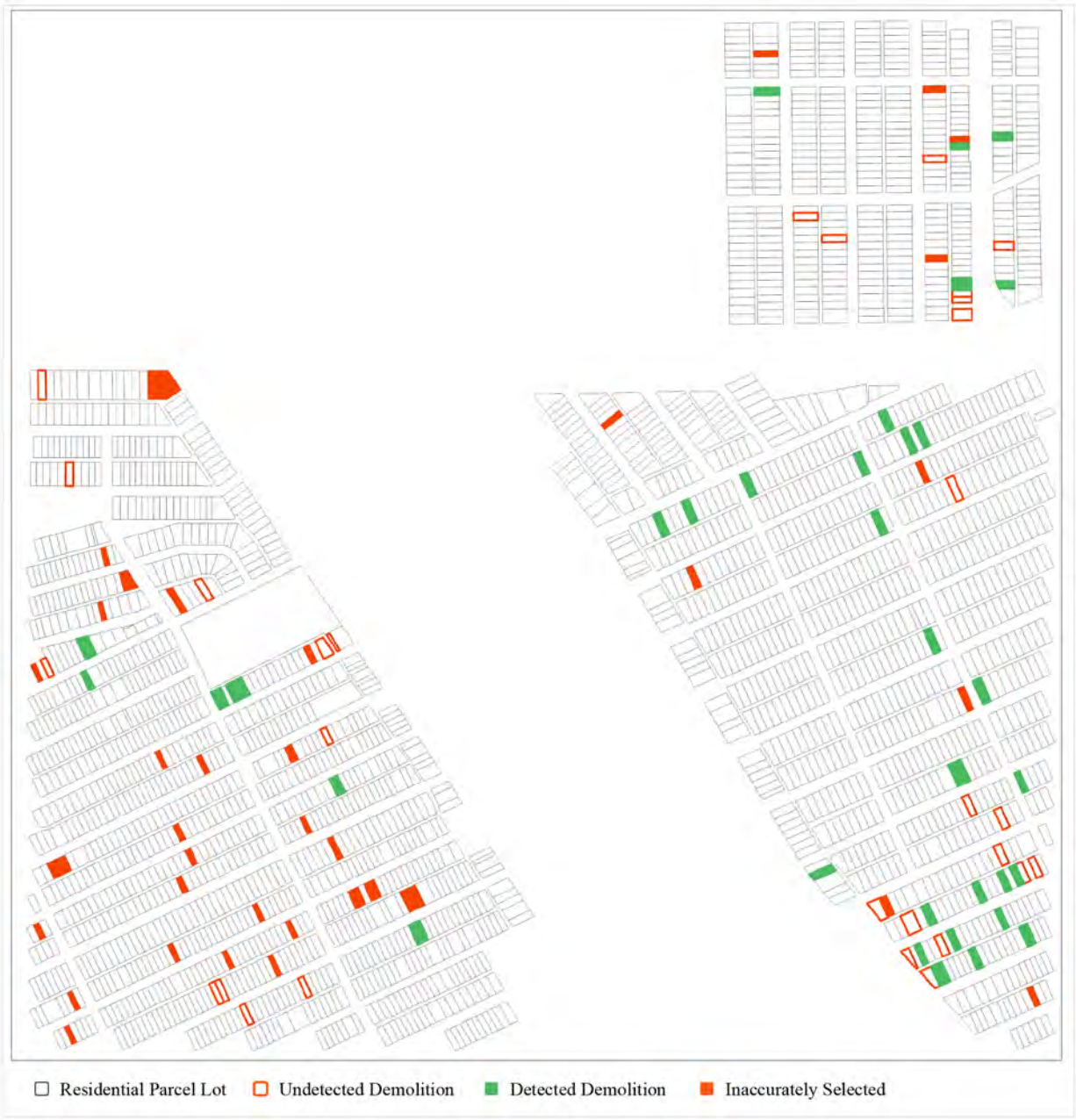

Figure 5.12: 2.59 square kilometre (one square mile) tile extent – correct/incorrect change detection (based on 25 square metre structure threshold)

Figure 5.13: Crary/St. Mary (low residential demolition rate) – correct/incorrect change detection (based on 25 square metre structure threshold)

Figure 5.14: Core City (median residential demolition rate) – correct/incorrect change detection (based on 25 square metre structure threshold)

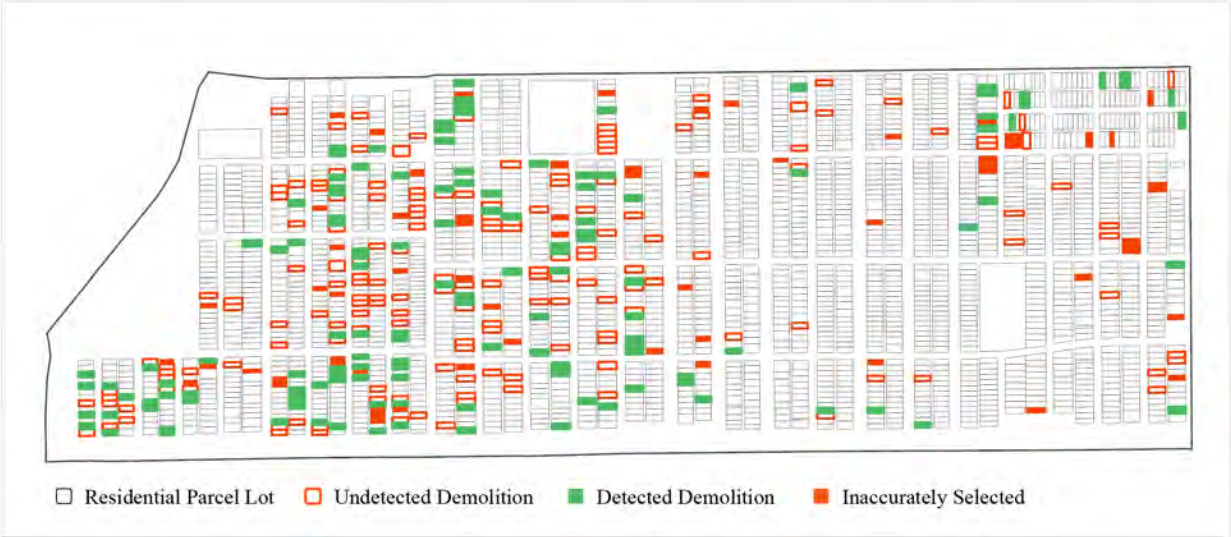

Figure 5.15: Pulaski (high residential demolition rate) – correct/incorrect change detection (based on 25 square metre structure threshold)

CHAPTER 6: Challenges, Conclusion, and Future Research

6.1 Challenges Encountered

"Change detection from remotely sensed data is a complicated process, with no single approach optimal and applicable to all cases" (Hussain *et al*., 2013). Many analyses face limiting factors, and this study is no different. Understanding potential points of friction can help future researchers be aware of what they may encounter, and what types of benefits can be extracted from the results. Each study faces a unique set of challenges based on by the data type, objective at hand, and/or methods. This study outlined several factors including data quality, consistency, and the challenges of using GEOBIA to solve the research questions that were posed.

6.1.1 Working with Aerial Photographs

While airborne imagery can provide higher spatial (pixel) resolution than publicly available satellite data, there are inherent factors that limit the quality of the imagery. The consistency of the sensor capturing the image, line of flight and altitude, time of day, meteorological conditions, and human processing techniques can all introduce variability to the final product. The challenge of sensor consistency is evident when working with NDVI values. The NDVI is not an absolute value, but rather a fraction of reflectivity ratio. Huang *et al*. (2020) demonstrated the difference of NDVI values when different sensors were used to capture the same ground features. In this study, the two NAIP imagery sets were captured with different sensors. NAIP imagery contains oblique views due to off-nadir capture angles, resulting in elevated features such as tree canopies appearing larger and over-representing true ground conditions (Toney *et al*., 2012). This type of error can compound when performing change detection analysis, as there is uncertainty concerning which features were impacted by the oblique view, as the flight line is not published by NAIP. Finally,

aerial photography does not penetrate through cloud cover or tree canopy, and consequently may not necessarily represent the ground surface. A human can read between the lines and infer a tree is covering a road, but it is much more complex to "teach" the computer to form this connection.

6.1.2 Current GEOBIA Limitations

GEOBIA has emerged as an alternative method to pixel-based analysis, with the promise of reducing or even erasing pixel-based method imperfections. Despite its potential, the GEOBIA field has yet to mature. For instance, the question of what parameter values to use for image segmentation is left nearly unanswered and to the discretion of the analyst, which often manifests in the form of multiple trials. While this allows for flexibility, it also introduces failure points.

GEOBIA methods overestimated tree canopy cover compared to human interpretation, often due to shadow misclassification (Toney *et al*., 2012). Surfaces are susceptible to lighting, view angles, and weather, which results in objects not appearing the same or having the same boundaries in different acquisition dates, even if they have not changed (Chen *et al.*, 2012).

Computational demands posed a challenge in this study's initial application of GEOBIA methods. When working with VHR 0.6m imagery, an initial 25 square kilometre tile was near impossible to process due to CATALYST becoming unresponsive. The training area was ultimately defined by computational capacity, possibly altering the overall results by restricting the variety of surfaces within the sample area. The computational demands of applying GEOBIA methods to large spatial extents were also acknowledged as an issue by Maxwell *et al*. (2019).

6.1.3 Objective Specific Challenges

In this study, three accuracy measures comprise the overall accuracy of the residential structure change detection: (a) the accuracy of the image segmentation/image-objects, (b) object classification accuracy, and (c) parcel classification (structure/no-structure). Despite good object classification accuracy, this does not translate to sufficient parcel change detection accuracy. Each one of the steps can imperil the accuracy of the change detection.

Liao *et al*. (2021), outlined the different spectral signatures of various rooftops, ranging from steel to brick, making the delineation of rooftops a complex process. Moreover, Chen and Hutchinson (2007) indicated that post-damage structures are more difficult to detect with OBCD than urban development. This poses a challenge with shrinking cities, as many of the structures that are demolished have sustained structural damage that prompted the demolition in the first place. Malanga (2009) indicated that houses are literally destroyed by vegetation overgrowth when they become vacant.

6.2 Conclusion

This study attempted to develop a workflow for identification of residential structure demolition in Detroit, a shrinking Rust Belt city. Experimentation with remotely sensed methods and GEOBIA workflows resulted in successful image segmentation and object classification that overcomes shadows. This study demonstrated that that it is possible to batch classify imagery in different areas of the city when captured by the same acquisition aircraft. This is significant, as processing VHR imagery requires high computational capacity, and working in smaller spatial extents may be necessary. It also demonstrated that classification of identical areas was possible when images were captured by various acquisition aircraft on different dates. By adjusting the

training objects and aligning them to near identical, the image segmentation and classification was performed successfully. *Pervious* and *Impervious* surfaces were successfully delineated despite the presence of heavy shadows. A single workflow was developed and applied with success.

Using 0.6 metre spatial resolution imagery, image segmentation was successfully performed when applied on the blue and NDVI channels, with a scale of 5, shape 0.1, and compactness 0.9. This combination generated different LULC boundaries under shadows. By using the mean values of all available CIR channels and the NDVI, the classification of *Pervious* and *Impervious* was most successful, with overall accuracy of over 98%. Due to computational demands when analyzing VHR imagery with GEOBIA methods, size and spatial extent play an integral role in the workflow.

Parcel classification into *structure*/*no-structure* based solely on *Impervious* land cover area yielded varying results. Successfully selected structures ranged between 63%-92%, where commission error ranged anywhere between 0.7%-82%. When the delineation of structures was performed in a neighbourhood with many vacant lots, the accuracy increased. The neighbourhoods with lower lot vacancies resulted in poorer delineation of structures on parcel lots. With the assistance of knowing where demolitions might have occurred, ground surveying resources can be assigned more efficiently. An approach that integrates visual interpretation is necessary to reliably detect changing residential demolitions within a shrinking Rust Belt city.

6.3 Recommendations for Future Research

Based on this research, this workflow can be repeated in a variety of locations which have a similar climate to Detroit by adjusting the training objects to represent the site's specific ground

conditions. The combination of spatial resolution and the geographic spatial extent should be considered, as those will impact the required computational capacity for the research.

Throughout this research several potential future investigation possibilities were identified. First, reducing data redundancy could assist when trying to segment the image for impervious surfaces. Algorithms such as Principal Component Analysis have been used in various other remote sensing applications, and early explorations in this study showed promising results. Second, because of the issues posed by shadows, it is more important to distinguish the areas under shadows to be certain of their surface. Clipping the image and performing additional GEOBIA on only the impervious surface can help ensure shadows are not misclassified into vegetative classes. Third, adding a 'bare soil' class may improve the impervious land surface area found on residential parcel lots with freshly demolished structures, since vegetation has not yet regrown on these parcel lots. Fourth, instead of addressing impervious land surface square metre area, intersect the generated areas from the two datasets. Perhaps more sophisticated mathematical equations could yield improved structure detection results. Finally, investigating the utility of performing year to year band-differencing, and segmenting those results could be considered.

Besides potential avenues to explore, some things should be kept in mind for future studies. Imagery with leaf-on conditions introduced multiple barriers when trying to detect rooftops, from roofs being covered by tree canopies, to vegetation consuming about-to-be-demolished residential structures.

REFERENCES

Ager, S. (2015). Taking back Detroit. *National Geographic*, 227(5), 56-83.

Biron, C. L. (2022). Feature: From stormwater to farms, U.S. cities put empty lots to use. *Reuters News Agency*. https://www.reuters.com/article/usa-cities-land-idUSL8N2U73AA Accessed: February 1, 2022.

Blaschke, T. (2010). Object based image analysis for remote sensing. *ISPRS Journal for Photogrammetry and Remote Sensing*, 65, 2-16.

Blaschke, T., Hay, G. J., Kelly, M., Lang, S., Hofmann, P. Addink, E., Feitosa, R. Q., van der Meer, F., van der Werff, H., van Coillie, F., and Tiede, D. (2014). Geographic object-based image analysis - Towards a new paradigm. *ISPRS Journal of Photogrammetry and Remote Sensing*, 87(100), 180-191.

Burkholder, S. (2012). The new ecology of vacancy: Rethinking land use in shrinking cities. *Sustainability*, 4, 1154-1172.

Byles, J. (2006). Disappeared Detroit. *LOST Magazine*. http://lostmag.matthewbrian.com/issue42/detroit.php#_ednref21

Chen, G., Hay, G. J., Carvalho, L. M. T., and Wilder, M. A. (2012). Object-based change detection. *International Journal of Remote Sensing, 33*(14), 4434-4457.

Chen, Z. Q., and Hutchinson, T. C. (2007). Urban damage estimation using statistical processing of satellite images. *Journal of Computing in Civil Engineering*, *21*(3), 187–199.

City of Detroit. (2021a). *Completed residential demolitions;* [Data set]. City of Detroit Open Data Portal. https://data.detroitmi.gov/datasets/detroitmi::completed-residential-demolitions/about Accessed: October 18, 2021.

City of Detroit. (2021b). *Parcels;* [Data set]. City of Detroit Open Data Portal. https://data.detroitmi.gov/datasets/detroitmi::parcels-2/about Accessed: September 15, 2021.

City of Detroit. (2021c). *Current City of Detroit Neighborhoods;* [Data set]. City of Detroit Open Data Portal. https://data.detroitmi.gov/datasets/detroitmi::current-city-of-detroit-neighborhoods/about Accessed: March 10, 2021.

Davis, D. (2017). *National Agriculture Imagery Program (NAIP) Information Sheet*. https://www.fsa.usda.gov/Assets/USDA-FSA-Public/usdafiles/APFO/support-documents/pdfs/naip_infosheet_2017.pdf

Data Driven Detroit. (2014a). *Motor City Mapping, Enhanced File (October 1st Survey Results)*; [Data set]. https://portal.datadrivendetroit.org/datasets/D3::motor-city-mapping-enhanced-file-october-1st-survey-results/about

Data Driven Detroit. (2014b). *Detroit parcel survey: Motor city mapping*. https://datadrivendetroit.org/files/DCPS/D3_NNIP_040414.pdf

Deng, C., and Ma, J. (2015). Viewing urban decay from the sky: A multi-scale analysis of residential vacancy in a shrinking U.S, city. *Landscape and Urban Planning*, (141), 88-99.

Detroit Data Collaborative. (2010). *Detroit Residential Parcel Survey*. https://datadrivendetroit.org/files/DRPS/Detroit%20Residential%20Parcel%20Survey%20OVERVIEW.pdf

Detroit Future City. (2016). *Achieving an integrated open space network in Detroit. Detroit Future City*. https://detroitfuturecity.com/wp-content/uploads/2015/06/DFC-Open-Space-Report-1.pdf

Ellis, E. A., and Mathews, A. J. (2019). Object-based delineation of urban tree canopy: assessing change in Oklahoma City, 2006-2013. *Computers, Environment and Urban Systems, 73,* 85-94.

Forsythe, K.W., and Waters, N.M. (2006). The Utilization of Image Texture Measures in Urban Change Detection. *Photogrammetrie-Fernerkundung-Geoinformation, (PFG 4/2006)*, 287-296.

Foster, A., and Newell, J. P. (2019). Detroit's lines of desire: Footpaths and vacant land in the Motor City. *Landscape and Urban Planning,* 189, 260-273.

Gibson, C. (1998). *Population of the 100 largest cities and other urban places in the United States: 1790 to 1990.* United States Census Bureau. https://www.census.gov/library/working-papers/1998/demo/POP-twps0027.html

Giner, N. M., Polsky, C., Pontius, R. G., and Runfola, D. M. (2013). Understanding the social determinants of lawn landscapes: A fine-resolution spatial statistical analysis in suburban Boston, Massachusetts, USA. *Landscape and Urban Planning, 111*, 25-33.

Goodman, A. C. (2004). *Detroit housing rebound needs safe streets, good schools*. https://allengoodman.wayne.edu/RESEARCH/PUBS/a09-87052.htm

Hartt, M. (2018). The diversity of North American shrinking cities. *Urban Studies*, 55(13), 2946-2959.

Hay, G. J, and Castilla, G. (2008). Geographic Object-Based Image Analysis (GEOBIA): A new name for a new discipline. In: Blaschke, T., Lang, S., and Hay, G. (eds.) *Object Based Image Analysis*, Springer, Heidelberg, Berlin, New York, 93-112.

Huang, S., Tang, L., P. Hupy, J., Want, Y., and Shao, G. (2020). A commentary review on the use of normalized difference vegetation index (NDVI) in the era of popular remote sensing. *Journal of Forestry Research, 32*(1), 1-6.

Hussain, M., Chen, D., Cheng, A., Wei, H., and Stanley, D. (2013). Change detection from remotely sensed images: From pixel-based to object-based approaches. *ISPRS journal of photogrammetry and remote sensing,80*, 91-106.

Hoalst-Pullen, N., W. Patterson, M., D., and Gatrell, J. (2011). Empty spaces: neighborhood change and the greening of Detroit, 1975-2005. *Geocarto International,* 26(6), 417-434

Hollander, J. B. (2011). *Sunburnt Cities*. New York, NY: Routledge.

Hossain, M. D., and Chen, D. (2019). Segmentation for Object-Based Image Analysis (OBIA): A review of algorithms and challenges from remote sensing perspective. *ISPRS Journal of Photogrammetry and Remote Sensing,* 150, 115-134.

Jayasekare, A. S., Wickramasuriya, R., Namazi-Rad, M., Perez, P., and Singh, G. (2017) Hybrid method for building extraction in vegetation-rich urban areas from very high-resolution satellite imagery. *Journal of Applied Remote Sensing, 11*(3)

Johnson, B. A., and Ma, L. (2020). Image segmentation and object-based image analysis for environmental monitoring: Recent areas of interest, researchers' views on the future priorities. *Remote Sensing, 12*(11), 1772.

Kinder, K. (2016). *DIY Detroit: Making do in a city without services*. Minneapolis, MN: University of Minnesota Press.

Lang, S., (2008). Object-based image analysis for remote sensing applications: Modeling reality-dealing with complexity. In: *Object-Based Image Analysis*. Berlin, Heidelberg, 3-27.

Liao, W., Deng, Y., Li, M., Sun, M., Yang, J., and Xu, J. (2021). Extraction and analysis of finer impervious surface classes in urban area. *Remote Sensing*, *13*(459).

Ma, L., Li, M., Blaschke, T., Ma, X., Tiede, D., Cheng, L., Chen, Z., and Chen, D. (2016). Object-based change detection in urban areas: The effects of segmentation strategy, scale, and feature space on unsupervised methods. *Remote Sensing,* 8(9), 761-779.

Makela, H., and Pekkarinen, A. (2001), Estimation of timber volume and the sample plot level by means of image segmentation and Landsat TM imagery. *Remote Sensing of Environment 77*, 66–75.

Malanga, S. (2009). Feral Detroit: Nature is reclaiming the Motor City. *City Journal*. Autumn 2009. https://www.city-journal.org/html/feral-detroit-13242.html

Maxwell, A. E., Strager, M. P., Warner, T. A., Ramezan, C. A., Morgan, A. N., and Pauley, C. E. (2019). Large-Area, high spatial resolution land cover mapping using Random Forests, GEOBIA, and NAIP orthophotography: Findings and recommendations. *Remote Sensing, 11*(12), 1409.

Maxwell, S. K. (2010). Generating land cover boundaries from remotely sensed data using object-based image analysis: Overview and epidemiological application. *Spatial and Spatio-Temporal Epidemiology, 1*(4), 231-237.

Mendiratta, P., and Gedam, S. (2018). Assessment of urban growth dynamics in Mumbai Metropolitan Region, India using object-based image analysis for medium-resolution data. *Applied Geography, 98*, 110-120.

Merry, K., Siry, J., Bettinger, P., and Bowker, J. M. (2014). Urban tree cover change in Detroit and Atlanta, USA, 1951-2010. *Cities, 41,* 123-131

Norman, M., Mohd Shahar, H., Mohamad, Z., Rahim, A., Amri Mohd, F., and Zulhaidi Mohd Shafri, H. (2021). Urban building detection using object-based image analysis (OBIA) and machine learning (ML) algorithms. *IOP Conference Series. Earth and Environmental Science, 620*(1), 12010.

Shahi, K., Shafri, H. Z. M., and Hamedianfar, A. (2017). Road condition assessment by OBIA and feature selection techniques using very high-resolution WorldView-2 imagery. *Geocarto International, 32*(12), 1389-1406.

Sidhu, N., Rishi, M. S., and Singh, R. (2016). Spatio-temporal study of the distribution of land use and land cover change pattern in Chandigarh, India using remote sensing and GIS techniques. In Raju, J. N. (Eds.), *Geostatistical and geospatial approaches for the characterization of natural resources in the environment* (785-789). Springer International Publishing, 2016.

Singh, A. (1989). Digital change detection techniques using remotely-sensed data. *International Journal of Remote Sensing, 10*(6), 989-1003.

The Economist Newspaper. (2017a). How the riots of 50 years ago changed Detroit. *The Economist*. https://www.economist.com/united-states/2017/07/27/how-the-riots-of-50-years-ago-changed-detroit

The Economist Newspaper. (2017b). In Detroit, the end of blight is in sight. *The Economist*. https://www.economist.com/united-states/2017/09/16/in-detroit-the-end-of-blight-is-in-sight

Thompson, E. S., and de Beurs, K. M. (2018). Tracking the removal of buildings in rust belt cities with open-source geospatial data. *Int J Appl Earth Obs Geoinformation*, 73, 471-481.

Toney, C., Liknes, G., Lister, A., and Meneguzzo, D. (2012). Assessing alternative measures of tree canopy cover: Photo-interpreted NAIP and ground-based estimates. In: McWilliams, Will; Roesch, and Francis A. eds. (2012). *Monitoring Across Borders: 2010 Joint Meeting of the Forest Inventory and Analysis (FIA) Symposium and the Southern Mensurationists.* e-Gen. Tech. Rep. SRS-157. Asheville, NC: U.S. Department of Agriculture, Forest Service, Southern Research Station. 209-215.

Tortini, R., Mayer, A. L., and Maianti, P. (2015). Using an OBCD approach and Landsat TM data to detect harvesting on nonindustrial private property in Upper Michigan. *Remote Sensing, 7*(6), 7809-7825.

United Nations, Department of Economic and Social Affairs, Population Division. (2019). *World Urbanization Prospects The 2018 Revision*. https://population.un.org/wup/Publications/Files/WUP2018-Report.pdf

United States Census Bureau (2020). *QuickFacts Detroit city, Michigan*. https://www.census.gov/quickfacts/fact/dashboard/detroitcitymichigan/POP010220

United States Census Bureau (2021). *Gazetteer Files*. https://www2.census.gov/geo/docs/maps-data/data/gazetteer/2021_Gazetteer/2021_gaz_place_26.txt

United States Department of Agriculture (2021). *NAIP Imagery*. https://www.fsa.usda.gov/programs-and-services/aerial-photography/imagery-programs/naip-imagery/

Wang, X., Liu, S., Du, P., Liang, H., Xia, J., and Li, Y. (2018). Object-based change detection in urban areas from high spatial resolution images based on multiple features and ensemble learning. *Remote Sensing, 10*(2), 276.

Xie, Y., Gong, H., Lan, H., and Zeng, S. (2018). Examining shrinking city of Detroit in the context of socio-spatial inequalities. *Landscape and Urban Planning*, 177, 350-361.

Yen, C., Stow, D.A., and Toure, S.I. (2020). A histogram curve-matching approach for Object-based image change analysis of urban land use. *GI-Forum, 8*(2), 160-174.